THE UNIVERSITY OF MICHIGAN

COLLEGE OF ENGINEERING
Department of Aeronautical and Astronautical Engineering
Aircraft Propulsion Laboratory

Final Report

DESIGN CONSIDERATIONS FOR ARC HEATED HYPERSONIC TUNNEL

P. M. Sherman
H. C. Early
W. N. Lawrence

UMRI Project 02953

under contract with:

Mathematical Sciences Division
Department of the Navy
Office of Naval Research
Washington 25, D. C.

July 1960

ACKNOWLEDGMENT

This research was supported by the United States Navy under Contract No. Nonr-1224(31), Task No. NR 061-108, monitored by the Office of Naval Research, Mechanics Branch, Mathematical Sciences Division. The support of this agency is gratefully acknowledged.

TABLE OF CONTENTS

	Page
LIST OF SYMBOLS	iv
1. INTRODUCTION	1
2. GENERAL DESCRIPTION	2
3. OPERATING CONDITIONS	3
4. FACILITY COMPONENTS	7
a. Building Arrangement for Installation	7
b. Arc Chamber	8
c. Nozzle	13
d. Test Section	14
e. Transition Section	14
f. Vacuum Tank	14
g. Vacuum Pumping System	15
h. Instrumentation	15
i. Diffuser	16
j. Power Supply	16
REFERENCES	22
APPENDIX A	A-1
APPENDIX B	B-1

LIST OF SYMBOLS

A	Cross sectional area
a	Speed of sound
E_o	Energy delivered to reservoir gas
h	Enthalpy
M	Mach number
p	Pressure
Re	Reynolds number
T	Temperature
u	Velocity
V	Volume of arc chamber
γ	Isentropic exponent
ρ	Density

Subscripts

o	Stagnation conditions
∞	Test section conditions
*	Throat conditions
os	Reference conditions, 1 atmosphere pressure at $273^{\circ}K$

1. INTRODUCTION

The rapid development of high velocity craft has greatly stimulated interest in the new gas dynamic phenomena which occur at the high temperatures generated in hypersonic flight. The chemical changes which occur affect the entire flow field around a body as well as the interaction with the solid surface boundary. There is a dearth of experimental data necessary for predicting these effects. This report deals with the initial considerations in the design and fabrication of an arc heated tunnel facility to obtain such data. This tunnel is now under construction.

In order to obtain very high velocities, a great deal of energy is required. This, in general, means that such a facility must be quasi-steady, at best. The main advantage of the arc-heated tunnel is the possibility of obtaining high stagnation temperatures at comparatively high pressures for relatively long run times. High pressures are particularly important because the extent of chemical non-equilibrium in the nozzle expansion is sensitive to pressure (for a given temperature).

2. GENERAL DESCRIPTION

The tunnel installation consists of a small motor coupled to a d.c. generator with a heavy flywheel, a coil, arc chamber, nozzle, test section, vacuum tank and vacuum pumps. An early artists' conception of the installation is shown in Figure 1 and an overall layout is shown in Figure 2.

The general operation is the same in principal as for any blowdown tunnel. The arc chamber is filled with gas to the desired density. The downstream section is evacuated by means of the vacuum pumps. The small motor then brings the generator rotor and flywheel up to speed and the generator is pulsed to deliver current to the coil. When the current in the coil reaches a maximum, the circuit is interrupted so that the magnetic field of the coil collapses and an arc is initiated across the electrodes in the arc chamber. The arc heats the gas in the chamber at constant volume, to the desired stagnation temperature and pressure. The diaphragm at the entrance to the nozzle throat then yields and the heated gas in the arc chamber is accelerated through the nozzle and test section, where it reaches a high velocity, and into the vacuum tank.

Design consideration of components are discussed in section 4.

3. OPERATING CONDITIONS

Unfortunately, cost is always a consideration in determining the limitations of a system. There are two major cost limitations in a high pressure "hot-shot" type of facility. One is the cost of delivering the electrical energy. The other is the cost of constructing a chamber for high pressures.

The cost of even a small high pressure chamber increases very rapidly for pressure above 60,000 psi. The construction of a chamber for pressures over 250,000 psi becomes questionable, let alone expensive since present day alloys have a yield, at best, of below 300,000 psi. New materials or a careful pre-stressing of a series of shells present costly possibilities. A maximum pressure of 80,000 psi represented a reasonable compromise, and is therefore, one limitation on our operating conditions.

The cost of supplying energy to the gas is related to the efficiency of the energy transfer process. One problem in this connection is the problem of the change in average electrical resistance of the gas with time. As the arc is initiated the gas in the arc column becomes ionized and therefore its resistance tends to be reduced. On the other hand the column tends to be reduced in cross section by a pinch effect which would tend to increase the resistance of the pinched gas. In the case of the co-axial electrode geometry the arc column also tends to be stretched out in length and rotate. This would, of course, make for an increase in resistance. There has been some experimental evidence (References 1&2) that an overall

average resistance of .02 ohms may be used as a very rough approximation. If the average resistance is less, a higher current will be required for the given energy transfer. [Some provision for this possibility has been made (see Appendix A).] Energy transfer to the gas of 2×10^6 joules appears reasonable and is therefore a second limitation on our operating conditions.

With a given amount of energy, test-section conditions depend primarily on the quantity of gas in the arc chamber and the extent the gas is expanded from reservoir to test-section. Required and limiting stagnation conditions were computed for a variety of free stream conditions. These computations were based on chemical equilibrium throughout (References 3 and 4). Isentropic quasi-steady flow was assumed. Values for the region of density above one hundred times standard were obtained by extrapolation. These values are therefore only approximate.

Free stream conditions were assumed for the computation, and stagnation enthalpy computed from $h_o = h_\infty + 1/2\ u_\infty^2$. Stagnation conditions were then determined from the mollier diagram from h_o and the constant entropy known from free stream conditions. From stagnation internal energy and density, limitating stagnation conditions for a maximum energy transfer of 2×10^6 joules and given arc chamber volumes were determined.

Figure 3 is an example of computed stagnation conditions necessary for one set of test-section conditions. This graph is for $T_\infty = 270^\circ K$. Since the ρ_∞ curves are also constant entropy curves, if T_∞ were approximately $108^\circ K$ all the constant ρ_∞ curves would shift to the left

approximately one, i.e. a factor of approx. 10 ρ_{o_s} change. Likewise, if T_∞ were approximately 680°K all the ρ_∞ curves would shift to the right approximately one. The velocity curves would not change much with change in T_∞ in this high velocity region.

Figure 3 also indicates the limit on stagnation conditions for energy transfer of 2×10^6 joules and arc chamber volumes of 60 in.^{3} and 240 in.^{3} The 240 in.^{3} limitation on stagnation conditions is the same as that for the transfer of approx. 500,000 joules with the approx. 60 in.^{3} volume. Of course, any set of conditions below the energy limit lines could be obtained by the transfer of less energy.

Figures 4 through 11 indicate the change in thermodynamic coordinates through an isentropic expansion for two sets of stagnation conditions. They are compared with an expansion based on an effective isentropic exponent of 1.2 and 1.4. These computations are based on a graphical integration and therefore are not very accurate and are quite tedius. It appears that these equilibrium conditions cannot be approximated by means of one effective isentropic exponent for the entire expansion. However, one exponent to some appropriate temperature, say 2000°K, and another for the remainder of the expansion appears feasible. For completely frozen flow the effective γ would be above 1.4 due to the presence of monatomic molecules. For flow where just composition is frozen, γ would approach 1.28 for diatomic molecules with vibrational degrees of freedom, or somewhat less where other degrees of freedom such as ionization enter. These have not been computed

partly because there is evidence (Reference 5) that at relatively high stagnation pressures the flow through a nozzle expansion will remain very close to chemical equilibrium.

Figures 4 through 11 are based on the method described in Reference 6. This method employs the mollier diagram and a graphical integration of the steady, one-dimensional momentum equation in the form $\frac{d(u^2/2)}{dp} = -\frac{1}{\rho}$. [T, a, and ρ are plotted versus p. Then $\frac{1}{\rho}$ is plotted versus p and graphically integrated to obtain $u^2/2$ as a function of p. u and M are obtained from $u^2/2$ and a respectively, and A/A*, from $\frac{\rho_* u_*}{\rho u}$. The calculations for the $\rho_o/\rho_{os} = 200$ conditions are based on extrapolated values.] Figure 12 is a plot of free stream Reynolds number per foot versus free stream Mach number for a few values of free stream temperature and density as parameters. These curves were computed on the same basis as Figure 3.

The usual quasi-steady state blowdown tunnel expression was employed to approximate the change of stagnation conditions with time, after flow is established. An arbitrary limit of approx. 1% decay in stagnation density per millisecond of flow time was employed. This limit for our initial short nozzle represents an average of approx. .3% decay in stagnation density per particle residence time in the nozzle.

The decay rate is a function of the ratio of arc chamber volume to throat size as well as a function of the stagnation conditions. Setting the decay rate for a given arc chamber volume places a maximum on the

throat size or a minimum on the test section velocity for a given effective test-section size. The effective test-section area depends on the boundary layer displacement thickness. Unfortunately there is no reliable way of determining the boundary layer displacement thickness. All present methods are of questionable accuracy. One added problem here is the extent that the nozzle wall provides effective boundary layer cooling in the short period of time involved. For T_∞ approx. 100°K and an effective test-section area of 1 square foot, the minimum velocity is limited to approx. 8000 ft/sec. At T_∞ approx. 270°K, this becomes approx. 13,000 ft/sec.

Run time is usually considered from the start of the flow in the test-section to the time of flow breakdown. (See Section 4 f.) From all indications, however, there is a time lag in the adverse temperature effects on the surfaces in the arc chamber. That is, erosion or evaporation of electrodes, liner, insulation, etc. increases rapidly with elapsed run time. The run time will therefore be limited by the opening of a valve in the arc chamber. (See Section 4 b.). This "dump valve" will limit the run time to 15 to 20 milliseconds.

4. FACILITY COMPONENTS

a. Building Arrangement for Installation

The tunnel is to be installed in an addition to the Aircraft Propulsion Laboratory. The general arrangement of the layout is as shown

in Figure 2. A special cavity and concrete pad with built in ties were constructed for the motor-generator-flywheel power supply. Completely isolated concrete pads are also included for model support and support of optical equipment. Floor pad provision has been made for the use of a schlieren system of long focal length. Support for the arc chamber is to be built into the floor.

The coil, electrodes, arc chamber, nozzle, and vacuum tank are on a common centerline. Steel has been kept to a minimum in the vicinity of the coil to minimize magnetic losses and field distortion.

b. Arc Chamber

Figure 13 shows the internal arrangement of the arc chamber. The main considerations in the design are: 1) maximum internal pressure, 2) maximum wall stress, 3) volume, 4) internal geometry, 5) electrode geometry, 6) nozzle-throat geometry, 7) pressure seals and insulation.

1) As previously indicated the design is based on a maximum internal pressure of 80,000 psi. The decision was largely a cost factor.

2) The maximum wall stress occurs at the inside surface of the chamber. It will always, of course, exceed the maximum pressure, no matter how thick the chamber wall is. Successful heat treatment of thick walls requires special alloys and these are expensive and difficult to machine. The wall thickness is determined by the maximum internal pressure, the material used and a factor of safety of 2. Thick

shell elasticity theory is used to determine stresses.

3) Choice of arc chamber volume is related to maximum energy transfer to gas, stagnation pressure and temperature limits, and the decay rate of stagnation conditions. For a given energy transfer, higher temperatures and pressures are possible with a smaller volume. (See Figure 3). The decay rate of stagnation conditions decreases as the volume increases. Therefore, it is desirable to have as large a chamber as possible from the one standpoint and as small a chamber as possible from the other standpoint. Once maximum stagnation pressure is determined for a given energy transfer, however, the arc chamber volume is roughly determined. This can be seen from Figure 3. For a pressure maximum of 80,000 psi and energy transfer of 2×10^6 joules, an arc chamber volume of 60 $in.^3$ was decided on as consistant with all requirements.

4) For a given volume, several arc chamber geometries are feasible. Volume to internal surface area should be a maximum for minimum loss due to heat transfer to the chamber walls. A maximum volume to surface area ratio would be obtained by a spherical chamber. However, a spherical chamber presents problems in fabrication and sealing. A cylindrical chamber was decided on to obtain axial symmetry, ease of fabrication and economy. For a cylindrical chamber a length to diameter ratio of approx. 1 is closest to the

sphere configuration. It is desirable, however, to allow for a long "stretched out" arc so that a length to diameter ratio of >7 1 has an advantage. The compromise of a length to diameter ratio of approx. 2 was made.

5) The electrode geometry should provide for good contacts at all junctions, reasonable current density, the possibility of varying the distance between electrodes, and uniform transfer of energy. Soft copper washers and silver plated surfaces are provided to minimize contact resistance between surfaces. Electrode diameter is kept at a minimum of 1-1/2" with no section having less than that equivalent area. There is evidence (Reference 7) that with co-axial electrodes, the arc rotates, resulting in a more uniform transfer of energy and less electrode evaporation. The electrode tips are therefore concentric. They are removable to provide for altering the distance between them.

6) The subsonic section of the nozzle, and the throat section, as well as a portion of the supersonic section of the nozzle are all part of the arc chamber structure. The entrance to the throat should be smooth and gradual. A total conical angle of 20° was chosen for this. The downstream section of the nozzle has a total angle of 15° (See Section 4 c.). The throat section must withstand high heat transfer rates. Tungsten throat inserts are used for this purpose. These inserts are made with a straight section at the throat of the

order of the throat diameter. There is evidence that such a design makes for a more uniform flow. Throat size to obtain given test section conditions depends on effective test-section area. This in turn depends on boundary displacement thickness. Until we know more about computing displacement thickness, throat size for given test-section conditions cannot be determined. Throat diameters will vary between approx. .02" and .15" as outside limits.

7) Most materials generally used for sealing purposes extrude at a pressure of 80,000 psi. Pressure sealing the arc chamber therefore becomes a problem. Seals must be designed so that there is no place for any extruded material to go. This is also true of electrical insulation materials. Here there are some exceptions, however. One is natural mica which can be "piled up" in thin sheets for insulation in the direction perpendicular to the sheets. Another is aluminum oxide porcelain which will take a compression load of over 200,000 psi. There is also malamine-glass insulation which is quoted as taking a compressive load of 90,000 psi. A combination of the mica and epoxy-glass has been used successfully (Reference 8).

8) A liner for the chamber is advisable for two reasons. It facilitates moderate changes in internal size and/or geometry. It also makes possible the use of a material of high thermal and electrical conductivity for the inside surface of the chamber. A perforated baffle is provided as part of the liner to provide somewhat of a

settling chamber and to smooth the fluctuations set up by the rotating arc. The baffle is placed in the chamber so that there is a comparatively small volume on the downstream side to minimize pressure lag on the downstream side of the baffle. The diaphragm is placed just upstream of the throat and can be either a plastic film such as Mylar or a scribed metal disc. The Mylar probably evaporates. The scribed metal has the advantage of rupturing at a given pressure.

9) Advantage can be taken of the time lag in the contamination of the gas by oxidation, evaporation and/or erosion of metal component in the arc chamber, by venting the arc chamber after a pre-set period of time. A large fast acting valve is required for this purpose. Two possibilities are being considered for this valve. One is an explosive charge in a plastic plug, the other is a closing based on explosive bolts. In either case automatic triggering by a timing circuit is required. The hot gas will be vented vertically through the roof to minimize the problem of reaction forces.

10) The arc chamber will be mounted on rails so that it can be moved along its axis, horizontally. This makes for easy access and easy removal of the downstream section of the nozzle.

c. Nozzle

The initial nozzle to be used is axisymmetric. An axisymmetric nozzle has the following advantages: 1) minimum throat perimeter to throat area ratio for minimum change in throat section with time, 2) smooth boundary layer growth, 3) greater flow uniformity, 4) symmetrical thermal expansion.

A conical nozzle was chosen for versatility and economy for initial operation. The nozzle has a total included angle of 15°. This represents a compromise between minimizing both axial gradients in the test-section and the possibility of boundary layer separation, and minimizing boundary layer displacement thickness. The larger the nozzle angle the greater the likelihood of boundary layer separation and the larger the gradients in the test-section. The smaller the nozzle angle the longer the nozzle becomes for a given test-section area and the thicker the boundary layer in the test-section.

For the high stagnation densities, the Reynolds number will be higher than the critical Reynolds number for the region in the nozzle where the flow reaches a Mach number of about 3. (Reference 9). The boundary layer will therefore probably become turbulent long before reaching the test-section region, so that even though the boundary layer is cooled it will probably be turbulent in the test-section region.

d. Test Section, e. Transition Section

There appears to be little advantage to a straight test-section with a conical nozzle. The test-section region is therefore in the conical portion of the tunnel. The diameter at the test-section centerline is approximately 19". A conical section downstream of the test-section has provision for model mounting and instrumentation access. The nozzle and test-section are in one piece and can be removed without interferring with any model mounting.

f. Vacuum Tank

The vacuum section downstream of the test-section has a volume of approximately 400 cubic feet. If a diffuser is employed, the vacuum tank should be large enough so that the pressure in the tank will not increase beyond that behind the normal shock at the diffuser exit, before the end of the run. A more conservative limitation is a tank large enough so that with the maximum mass flow, the pressure in the tank does not reach the test-section exit pressure before the end of the run. Both criteria were considered in determining the vacuum tank volume. The tank is 4 feet in diameter made in two sections for easy diffuser mounting, possible future change in test-section, and economy. Double welds are used for strength with the space between them vented to the vacuum side. This is done in order to minimize the possibility of virtual leaks from enclosed pockets. Single Army-Navy standard "O"-rings are employed for vacuum seals. Shell

thickness is based on ASME code with sections 3/8" and 5/16" thick. All inside surfaces are coated with low vapor pressure paint or oil to minimize the problem of removal of moisture from hygroscopic surfaces.

g. Vacuum Pump

To obtain proper starting of the flow through the nozzle a low pressure is required downstream of the nozzle so that the starting shocks will be swept rapidly downstream. (See Reference 10). An analysis of the starting problem requires a compressible two-dimensional unsteady solution for which no mathematical techniques are available. Some analyses, however, have been made by means of one-dimensional method of characteristics (Reference 10). Our vacuum system is based on obtaining a pressure of approximately 1/2 micron of mercury in less than an hour. Pumping performance is indicated in Figure 14. The system consists of a small rotary pump plus a 10" diffusion pump with necessary by pass and valves. A safety check is provided on the system by means of a relay for automatic valve closing in case of a pressure rise.

h. Instrumentation

Initially "standard" instrumentation will be employed for making measurements. Both a crystal type (Kistler) and a strain gage type (Norwood) of pressure transducer will be employed to obtain the stagnation chamber pressure. Variable reluctance gages will be employed to obtain lower pressures.

Photographs will be taken of the luminous flow field by means of a Fastax camera. This camera has been used to record at 7000 frames per second. It will also be used for future schlieren pictures.

i. Diffuser

Initially the diffuser will be omitted (for economy). The advantages of a diffuser apply here as in any blowdown tunnel. A conical section with an angle similar to that of the nozzle will probably eventually be used. It may be fabricated of a non-metalic material.

j. Power Supply

General Scheme - The power source for supplying electrical energy to the arc chamber is designed to store energy taken from the power line over a time interval of approximately 20 minutes and deliver it to the arc chamber during an interval of approximately 5 milliseconds. This energy will be stored by means of a d.c. unipolar generator and flywheel used in conjunction with a large inductance coil. The energy will first be stored in the flywheel over a 20 minute interval required for the flywheel to reach a speed of 10,000 rpm; then it will be transferred to the inductive energy storage coil over a 3 second interval and then transferred to the arc chamber during a 5 millisecond interval. (Reference 11).

Allis-Chalmers Unipolar Generator, Flywheel, and Drive Motor - The operation of the system is schematically shown in Figure 15. The generator

and flywheel are driven up to speed by the electric motor. Then, the field of the generator is energized by closing S_1, and the current builds up in the inductance coil. At the instant of current maximum, S_2 is opened, and the current is diverted to the arc chamber. The unipolar generator has been developed by the Allis-Chalmers Company for applications requiring very large amounts of low voltage d.c. current. For pulse operation, this generator runs at 10,000 rpm and will deliver 500,000 amperes at 45 volts. The generator does not use conventional brushes but uses liquid metal to make electric contact with the spinning rotor. The liquid metal is an eutectic mixture of sodium and potasium known as NaK which is liquid at room temperature. The flywheel has a diameter of 26 inches. At 10,000 rpm, the stored kinetic energy of the flywheel and generator rotor is 20 million joules.

Inductance Coil - The energy storage coil will have an inductance of 120 microhenries and a resistance of 47 microhms. The computed total circuit resistance, including the internal resistance of the generator, will be 65 microhms. This computation is based on published data regarding the resistance of bus bar connections and switch terminals. The computed energy storage in the magnetic field of the inductance is 6×10^6 joules at a current of 315,000 amperes. This current maximum will be reached approximately 3.2 seconds after the current starts to build up in the coil. There is some uncertainty regarding the time constant of the field winding of the unipolar generator. The rate of field build up is not accurately known under conditions where the generator is heavily loaded, and if the field time constant is longer

than expected, the maximum current may be somewhat less than 315,000 amperes.

Figure 16 is a plot of the generator current as a function of time. The first curve is based on the assumption that the field build up time is zero, while the second curve is based on the assumption that the generator field builds up at an exponential rate with a time constant of one second. The dotted portions of the two curves represent the circuit behavior if the firing switch were not opened at the time of the first current maximum. The electrical behavior of this circuit can be simplified by replacing the generator and flywheel with an equivalent capacitance of 20,000 farads charged to 45 volts. This is a good equivalent circuit for situations in which the rise time of the generator field is not significant.

The frame for the coil will be supported by a structure of heavy oak timbers. A photograph of this structure is shown in Figure 17. Although the total weight of the aluminum cable is only 15,000 lbs., the magnetic forces on this structure are quite large, and very heavy bracing is necessary to withstand these forces. The aluminum bus bars connecting the coil, switch, and generator will have a current-carrying cross-sectional area of 4" x 20". The coil winding will consist of 26 parallel conductors of polyethylene-insulated aluminum cable. Each conductor is 2" in diameter and has a cross-sectional area of 3,000,000 circular mils.

Appendices A and B describe design criteria and method of calculation of transient load current.

Switching - An optimum switching system for transferring the coil current into the arc chamber will need to interrupt a current of 300,000 amperes and withstand voltages up to 20 kilovolts within about a millisecond after the current is transferred. This is a very special switching requirement which cannot be met by commercially available switch gear. This switching problem can be greatly simplified if the arc inside the chamber is initiated by a heavy shorting wire (bar) which bridges the electrodes during the switching process. However, the vaporization of a shorting bar adds a substantial amount of contamination of the gas in the arc chamber, and it will be desirable to develop a switching arrangement which will permit the arc to be initiated with a minimum of gas contamination due to vaporized metal.

Present plans are to accomplish the switching in a 3-stage process which will use 2 switches and a fuse all connected in parallel. The #1 switch will be very heavy and massive and will carry most of the current during the 3 second charging interval. When this heavy #1 switch is opened, the current will be transferred to a lighter, faster acting switch which will carry the current for perhaps 1/10 second so that the heavy #1 switch has time to get completely open and deionized. The relatively light #2 switch will be opened by compressed air and by magnetic forces. It is expected that the opening time of #2 switch can be limited to about 2 milliseconds. The #2 switch will be shunted by a high voltage fuse which will carry the current for about 1 to 3 milliseconds before blowing and opening the circuit and thus diverting the current into the arc chamber.

Opening a circuit of this type has been accomplished at lower current levels in previous work at the University of Michigan. This previous work involved currents of about 5,000 amperes, and the fuse voltage would rise to 50 kilovolts in less than a millisecond. The fuse element consisted of a #18 copper wire inside a thick 1/4" I.D. fiberglass tube filled with oil. It is expected that this fuse technique using multiple fuse elements connected in parallel can be extended to the present application.

Under certain conditions the arc may not be successfully initiated in the arc chamber. To prepare for this possibility, two safety precautions are being provided. An overvoltage spark gap across the terminals of the energy storage coil will be adjusted to breakdown and short-circuit the coil at a maximum voltage of approximately 20 kilovolts. This overvoltage spark gap will be of extra heavy construction so that the elctrodes will not burn away if most of the stored energy is dumped into this arc. Another hazard is that the stored energy may be dissipated in the fuse box, and thereby generate a substantial explosion. The fuse will be located inside a thick walled concrete box filled with sand. One side of this box will consist of a plywood panel which will break in case of an explosion and vent the gas and sand outside the building.

The heavy #1 switch does not appear to involve any unusual design problems. For the #2 fast acting, mechanical switch, a variety of designs have been considered. After evaluating various alternative designs, it has been decided to build this switch in the form of a metal disk which

forms a low resistance short circuit across the end of a coaxial line. The shorting disk will be clamped in place by an explosive bolt assembly, and a 100 psi air tank will supply air pressure inside the coaxial line. When the switch operates, the bolt explodes, and the air pressure and magnetic force accelerate the shorting disk forward. The air flow assists in restraining the tendency of an arc to form across the switch terminals.

Sequence Timer - The firing of the tunnel will be carried out by an automatic timing mechanism. This sequence timer will program the following events: (1) applying pulsed pressure to the liquid metal (NaK) current collector system of the generator, (2) energizing the field of the generator to initiate the build up of current in the energy storage coil, (3) providing signals for starting recorders and triggering oscilloscopes, (4) opening the mechanical switches in the charging circuit, (5) energizing the suicide field reducing circuit on the generator, and (6) operating the dump valve which removes the residual gas in the arc chamber after the useful running time of the tunnel has been completed.

REFERENCES

1. Perry, R. W. and MacDermott, W. N., "Development of the Spark-Heated, Hypervelocity, Blowdown Tunnel-Hotshot", AEDC-TR-58-6, June 1958.
2. Turner, T. E., "Design of Lockheed Spark-Heated Wind Tunnel", LMSD-48467, March 1959.
3. Hilsenrath, J. and Beckett, C. W., "Tables of Thermodynamic Properties of Argon-Free Air to 15,000^{o}K" AEDC-TN-56-12, September 1956.
4. Feldman, Saul, "Hypersonic Gas Dynamic Charts for Equilibrium Air", AVCO, January 1957.
5. Hall, J. G. and Russo, A. L., "Studies of Chemical Nonequilibrium in Hypersonic Nozzle Flows", presented at Combustion Institute Meeting, Western States Section, Los Angeles, November 2-5, 1959.
6. Bird, G. A., "Some Methods of Evaluating Imperfect Gas Effects in Aerodynamic Problems", Royal Aircraft Establishment, January 1957,AD-139148.
7. Harris, W. G., "The Boeing Eight Inch Model Hotshot Wind Tunnel", D2-4711, September 1959.
8. Rohtert, R. E., Chief of Wind Tunnels, McDonnell Aircraft Co. - private communication.
9. Reshotko, Eli, "Stability of the Compressible Laminar Boundary Layer" Guggenheim Aeronautical Laboratory, Memo. No. 52, January 15, 1960.
10. Glick, H. S., Hertzberg, A., Smith, W. E., "Flow Phenomena in Starting a Hypersonic Shock Tunnel", AEDC-TN-55-16, March 1955.
11. Early, H. C. and Walker, R. C., "Economics of Multimillion-Joule Inductive Energy Storage", Communication and Electronics, No. 3, July 1957.

APPENDIX A

Design Criteria for the Energy Storage Power Source - Choosing the optimum design parameters for the power supply requires a knowledge of (1) the amount of energy to be delivered to the gas, (2) the rate of heat loss from the gas, (3) the efficiency of converting stored electrical energy to internal energy of the gas, and (4) the voltage and current characteristics of the arc as a function of gas temperature and pressure. Reasonable estimates are available as to the energy requirements. Estimates as to the voltage and current characteristics of the arc are based on extrapolations of arc characteristics under substantially lower pressures and temperatures. Because of this uncertainty, it is desirable to provide a maximum amount of flexibility in the design of the power supply. Additional flexibility will also be obtained by providing for possible modifications of the electrode geometry inside the arc chamber.

The choice of design values for the power supply was to a certain degree dictated by the characteristics of the Allis-Chalmers Model 2112 unipolar generator which was the only suitable choice commercially available. The generator peak current rating of 500,000 amperes places an upper limit on the pulse current obtainable from the power supply. The flywheel kinetic energy storage of 20,000,000 joules places a second limiting condition on the design of the system. In considering the optimum design of the inductance coil to operate with this generator, it was necessary to consider the relative importance of maximum energy storage vs. maximum current.

Calculations indicate that an energy storage of approximately 6 megajoules in the coil at 315,000 amperes could be obtained with a total circuit(d.c.) resistance of 65 μohms and an inductance of 120 μh. Of this 65 μohms total, 47 μohms will be in the coil and the remaining 18 μohms is the estimated resistance of the rest of the circuit including the switch and the internal resistance of the generator. However, the internal resistance of the generator is not known with any certainty, and if the actual resistance should be in error by 10 or 20 μohms, the wind tunnel design objectives could still presumably be met. On the other hand, a coil design which would attempt to utilize the full 500,000 ampere capability of the generator would involve more risk because (1) the total circuit resistance would need to be so low that any error in estimates would be very serious; (2) the inductance would be reduced by more than 50 per cent, and this could not be increased except by building a new coil; and (3) the time and cost of developing a 500,000 ampere switching system are substantially greater than for a 300,000 ampere system.

It was decided to go ahead with the 300,000 ampere design and build an inductance coil with a six-turn winding. If it is determined in the future that it is very important to go to higher currents, then one or two turns can be removed. Removing one turn will decrease the inductance by approximately 30 per cent and increase the peak current by about 20 per cent.

If it is assumed that the arc load behaves as a linear resistance of .02 ohms, the six-turn, 120 μh coil has a discharge time constant of 6×10^{-3} seconds. In the event that the arc resistance is less than the above figure and the discharge time is undesirably long, it may be desirable to use a

shorting switch across the electrodes to "chop off the tail" of the discharge pulse.

Choice of Conductor Size and Coil Dimensions - The total weight of aluminum used in the coil windings and bus bar connections was determined from economic considerations and the law of diminishing returns. Because of the very low duty cycle, the ohmic heating of the conductor is unimportant, and the use of extra parallel conductors serves only to reduce circuit resistance and increase the efficiency of energy transfer. The 26 parallel aluminum conductors used in the six-turn coil weigh 15,000 pounds and cost approximately $9,000. Extra expenditure to decrease the coil resistance would have increased the energy storage and peak current capability. However, the same increase in performance could be obtained at about the same cost by increasing the size of the flywheel. The choice of 15,000 pounds of conductor in the coil appears to represent a reasonable balance between the cost of the d.c. generator and the cost of the inductance coil as discussed in Reference 11.

In choosing the type and size of conductor, a comparison of costs indicated a substantial saving in using aluminum instead of copper. The use of 2" diameter 3,000,000 circular mil cable is advantageous compared to the use of a smaller size cable in that less space is lost in insulation and the more compact winding has a higher ratio of inductance to resistance. Still larger cable, up to 5,000,000 circular mils, could also have been obtained, and this was seriously considered. It was decided that the increased

difficulty in handling larger cable and in obtaining terminations of sufficiently low resistance would offset any advantages.

In order to minimize the high voltage insulation problem, all the 26 conductors have one common terminal on the inside (small radius) surface of the coil and another common terminal on the outside (large radius) surface of the coil. Aluminum clamping posts for terminating the inner ends of the coil winding can be seen in the photograph Figure 17. For design purposes, it is assumed that voltage spikes as high as 20 kv may be encountered. The voltage between any two adjacent turns will be only 1/6 of this total.

An overvoltage protector spark gap will be used to protect the system against excessive voltages. Since there may be arc-over conditions where several megajoules of stored energy has to be dissipated, arcing horns will be used to protect the gap from melting. The gap and horns will be located so that the magnetic field of the coil will act to move the arc along the horns. If preliminary tests indicate that an arc reaching the ends of the horns does not have enough voltage to re-ignite at the gap, this design will require modification.

The ratio of a.c. resistance to d.c. resistance of an inductance coil can be substantially reduced by (1) enameling the individual strands of the conductor, (2) transposing the winding in such a manner that all the parallel conductors have the same flux linkages and hence the same $\frac{d\phi}{dt}$ during the discharge. These refinements are of particular importance in the design of 60 cycle electrical equipment where the efficiency of power transformation is important, and power loss presents a cooling problem. In the design of

the present inductance coil, heating is not a factor and the loss of stored energy (of the order of 10 per cent) due to high a.c. resistance does not justify the added expense of using enameled wire and transposing the windings. Enameled aluminum wire costs two to three times the cost of bare aluminum wire and the problems associated with transposing the windings are complicated by the high magnetic forces on all the conductors.

The winding has a radial depth of 27 inches, an axial length of 31 inches and an average diameter of 120 inches. For a given length of wire, the optimum geometry of a winding for maximum inductance is when the radial thickness and the axial length of a winding are equal and 0.66 times the average diameter. The present coil has an inducatance of 95% of the inductance that could have been obtained by using the maximum inductance geometry. However, the larger diameter design has the advantage that the magnetic pinch force tending to compress the windings and stress the terminals is substantially reduced. Also the a.c. resistance loss due to parasitic eddy currents in the conductors is less than in the maximum inductance geometry.

APPENDIX B

Calculation of Transient Load Current of Generator - During the 20 minute interval required to run the generator and flywheel up to full speed, there is of course no electrical load on the generator. After the desired rotational speed has been reached, the build up of current in the generator and coil could be initiated by closing a switch in this circuit. However, such a switch would be very heavy and expensive and would have significant resistance. Hence, it is advantageous to omit the switch and initiate the load current by energizing the field winding of the generator.

The output voltage of the generator is given by the simple relation

$$E = K \phi n \qquad (1)$$

where ϕ = the total magnetic flux

n = rotational speed, taken here in revolutions per sec.

K = constant of proportionality

If the flux were to rise instantaneously, the voltage would be a step function, and the circuit could then be analyzed as a function of speed and current. In fact, under these conditions, the generator will behave exactly as if it were a 20,000 farad capacitor, and the analysis follows the conventional analysis for a series RLC circuit. Such an analysis has been carried out and is plotted in the first curve on Figure 16.

However, the field windings are inductive, and when the voltage is applied to the field winding, there is a time lag before the field current,

as the flux, reaches peak value. The exact manner in which the flux rises is a difficult problem in flux diffusion through iron and other conductors. The rate of flux rise is a function not only of the applied voltage but also of the load current the generator is delivering. The manufacturer estimates that the field will rise in the order of a second, although this has not been verified experimentally for large load currents. This is not negligible compared to the two second time constant of the energy storage coil. If it is assumed that the field flux will rise on an exponential path with a time constant of one second, the differential equations describing the voltage, current, and speed relations are given below.

First, the loop voltage equation is

$$L \frac{di}{dt} + R\, i = K \phi\, n \tag{2}$$

and if it is assumed that

$$\phi = \phi_m \left(1 - e^{-t/\tau}\right) \tag{3}$$

where τ is the time constant of the flux rise, here taken as one second, then by the conservation of energy, the total initial energy, W, at any later time must be the sum of stored inductive energy, the integral of the ohmic power losses and the remaining kinetic energy in the generator. Thus

$$W = \frac{1}{2} L\, i^2 + \int R\, i^2 d\, t + \frac{1}{2}\ I\ \omega^2 \tag{4}$$

where

$\omega = 2\, \pi\, n$

I = moment of inertia of the generator and flywheel.

Since the total energy is constant, the time derivative is zero.

Differentiating equation (4) after substituting in terms of n instead of ω yields

$$\frac{dW}{dt} = 0 = L\, i \frac{di}{dt} + R\, i + (2\pi)^2\, I\, n \frac{dn}{dt} \qquad (5)$$

Since the speed is decreasing ($dn/dt < 0$), the last term is negative, which may be interpreted as meaning that the power into the coil, plus the power into heat, is the power out of the generator. If the voltage equation (2) is multiplied by current, it becomes a power equation also.

$$i\, L \frac{di}{dt} + i\, R\, i = i\, K \phi\, n \qquad (6)$$

Subtracting (5) from (6) yields the differential relation between speed and current.

$$i\, K \phi\, n = -\, (2\pi)^2\, I\, n \frac{dn}{dt} \qquad (7)$$

or

$$i = \frac{-\,(2\pi)^2\, I}{K \phi} \cdot \frac{dn}{dt} \qquad (7a)$$

If the flux ϕ is independent of time, equation (7a) can be rewritten as

$$\int i\, d\, t = \frac{-\,(2\pi)^2 I}{K \phi}\, n \qquad (8)$$

and equation (2) becomes

$$L \frac{di}{dt} + R\, i + \frac{(K \phi)^2}{(2\pi)^2\, I} \int i\, d\, t = 0 \qquad (9)$$

If the coefficient of the last term is arbitrarily written as

$$\frac{(K \phi)^2}{(2\pi)^2\, I} = \frac{1}{C},$$

the relation to the standard RLC series circuit is immediately obvious. By way of comparison, the equivalent value of this capacitance is about

20,000 farads. The solution of equation (9) is relatively simple.

However, if the flux is not a constant but is given as a function of time as in equation (3), then while equation (7a) is valid, equation (8) is not. It is possible to differentiate equation (7a) and substitute back into the voltage equation (2) yielding a single differential equation in n. The equation, while linear, does not have constant coefficients. To add to the difficulty, the singular points of the differential equation are essential singularities, and, thus, will not yield to a power series solution.

A numerical solution must be obtained, however, which yields the current as a function of time. Using three equations,

$$L \frac{di}{dt} + R\, i = K \phi\, n$$

$$\phi = \phi_m (1 - e^{-t})$$

and $W = \frac{1}{2} L\, i^2 + R\, i^2\, d\, t + \frac{1}{2} I (2\ )^2\, n^2,$

a simultaneous solution for current and speed was obtained. The current has been plotted in Figure 16.

There is not much difference in the peak value of coil current whether the flux rises rapidly or in about one second. The reason for this is that most of the energy dissipation occurs when the current is near maximum value. During the time when the flux is low, the current is also low, so that the net result is that energy loss is low. For example, at 1.5 seconds, half the time to reach the peak current, less than 5 per cent of the total energy has gone into heating. By the time that the

current reaches peak value, about 60 per cent of the energy has gone into heating.

If the assumption of a one second time constant for the flux rise is valid, the time delay of flux rise is not too important. Its primary effect is to extend the time necessary to reach peak current, but it does not cause appreciable energy loss. If, however, the rise time is substantially longer, a high current switch between the generator and the coil may be required.

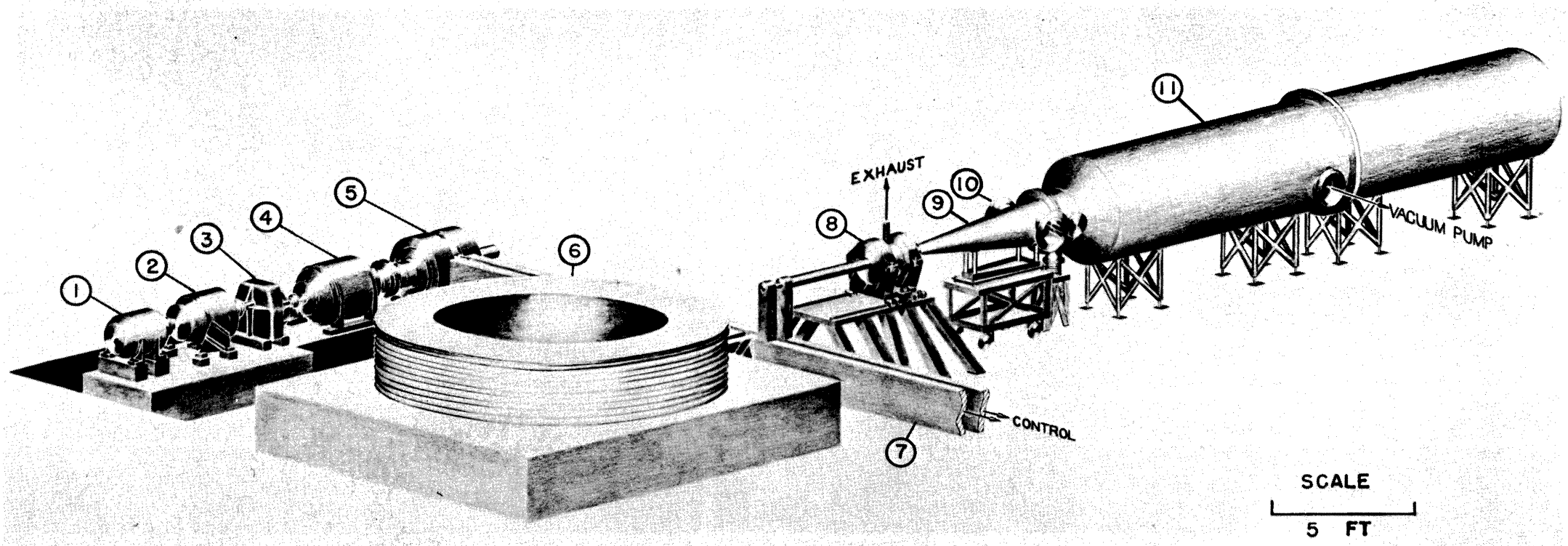

(1) 75 HP MOTOR
(2) DYNAMATIC MAGNETIC COUPLING
(3) SPEED INCREASER GEARBOX
(4) FLYWHEEL
(5) UNIPOLAR GENERATOR
(6) COIL
(7) BUS-BARS TO SWITCHES AND FUSES
(8) ARC CHAMBER
(9) NOZZLE
(10) TEST-SECTION
(11) VACUUM TANK

FIG (1)

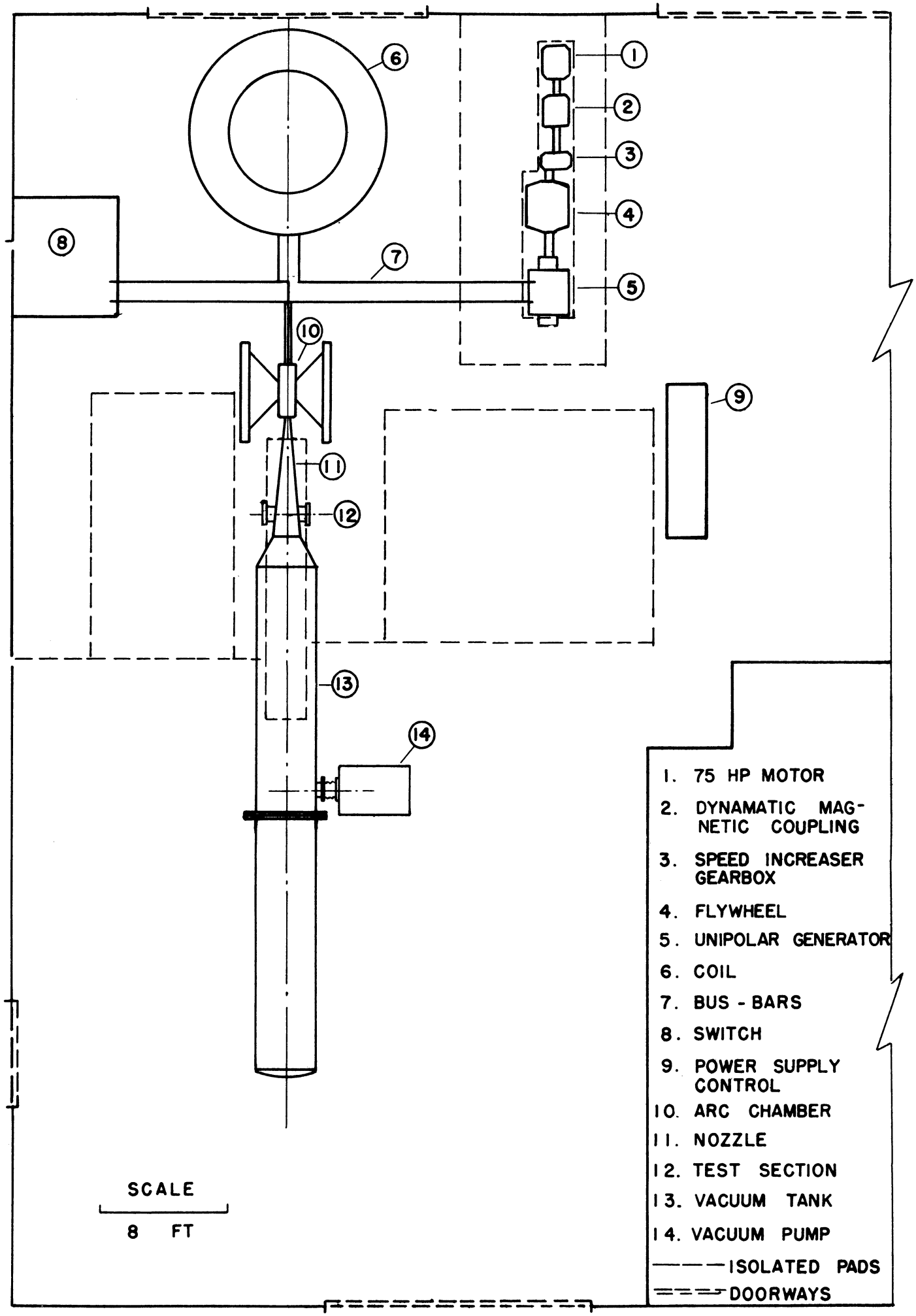
1. 75 HP MOTOR
2. DYNAMATIC MAG-NETIC COUPLING
3. SPEED INCREASER GEARBOX
4. FLYWHEEL
5. UNIPOLAR GENERATOR
6. COIL
7. BUS - BARS
8. SWITCH
9. POWER SUPPLY CONTROL
10. ARC CHAMBER
11. NOZZLE
12. TEST SECTION
13. VACUUM TANK
14. VACUUM PUMP
ISOLATED PADS
DOORWAYS
SCALE
8 FT

FIG (2)

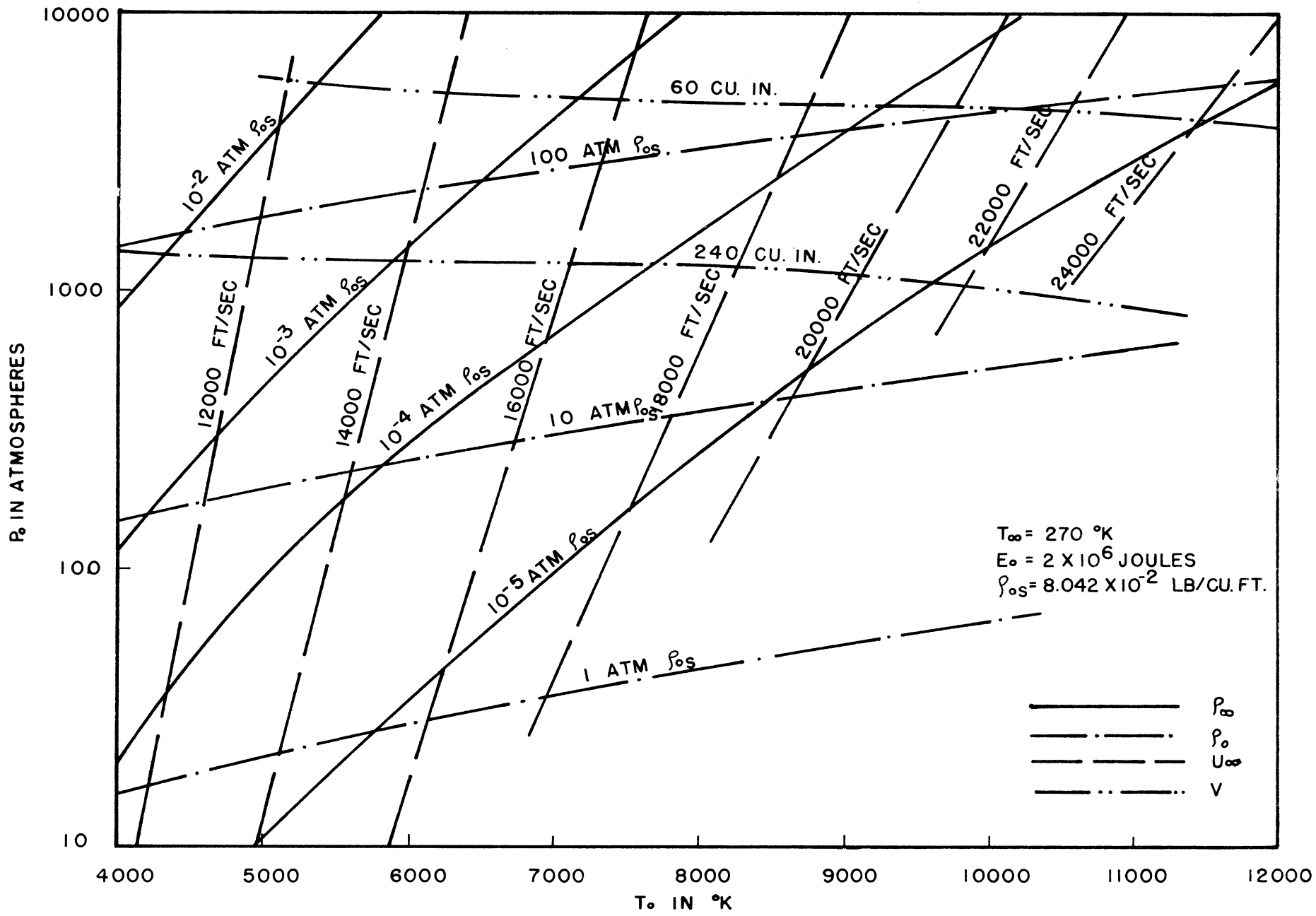
10000
1000
100
10
P_0 IN ATMOSPHERES
60 CU. IN.
240 CU. IN.
10^{-2} ATM ρ_{os}
100 ATM ρ_{os}
10^{-3} ATM ρ_{os}
10^{-4} ATM ρ_{os}
10 ATM ρ_{os}
10^{-5} ATM ρ_{os}
1 ATM ρ_{os}
12000 FT/SEC
14000 FT/SEC
16000 FT/SEC
18000 FT/SEC
20000 FT/SEC
22000 FT/SEC
24000 FT/SEC
T_∞ = 270 °K
E_0 = 2 X 10^6 JOULES
ρ_{os} = 8.042 X 10^{-2} LB/CU. FT.
ρ_∞
ρ_0
U_∞
V
4000
5000
6000
7000
8000
9000
10000
11000
12000
T_0 IN °K

FIG (3)

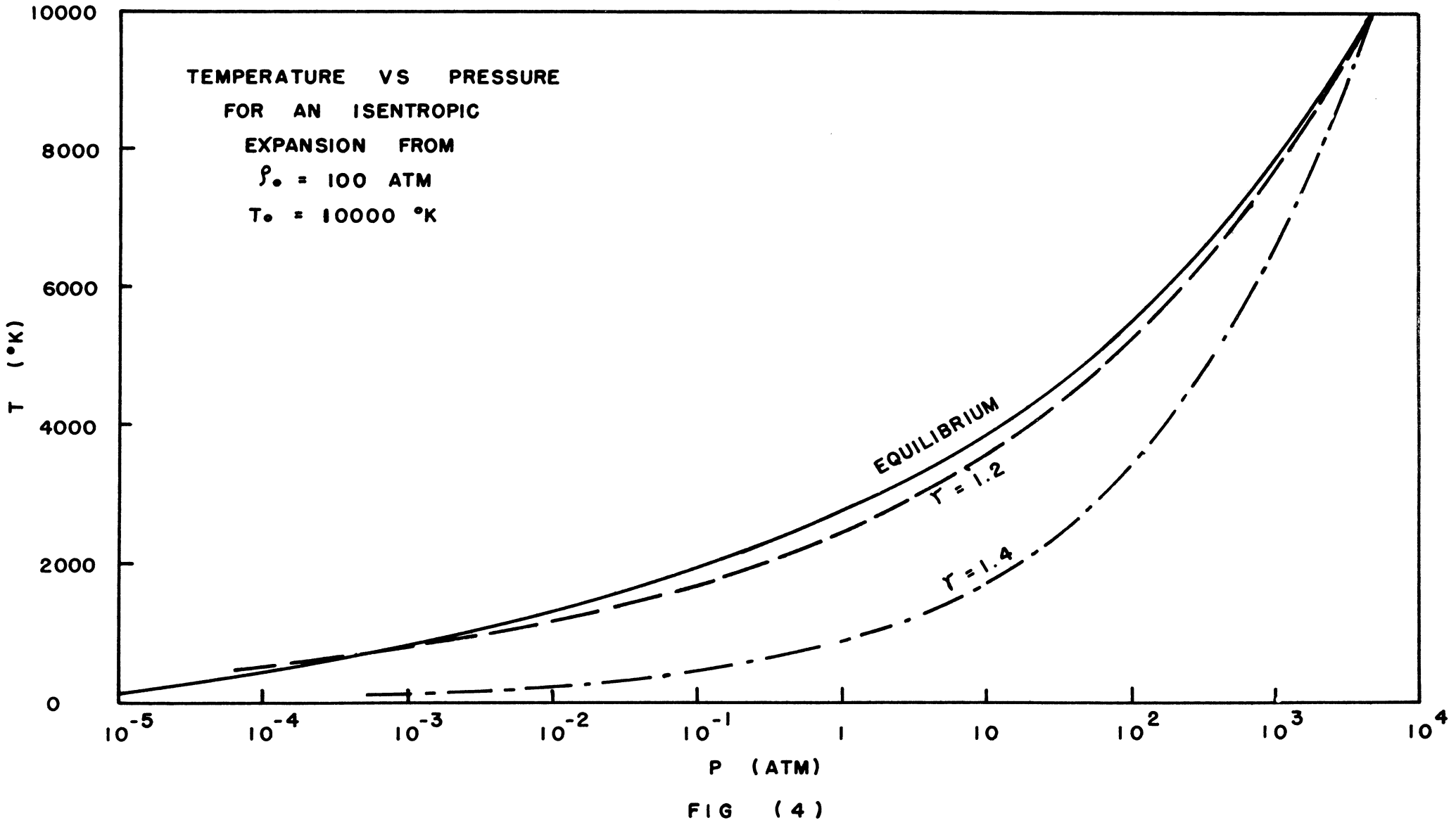
TEMPERATURE VS PRESSURE
FOR AN ISENTROPIC
EXPANSION FROM
ρ_o = 100 ATM
T_o = 10000 °K
EQUILIBRIUM
γ = 1.2
γ = 1.4
T (°K)
10000
8000
6000
4000
2000
0
10^{-5}
10^{-4}
10^{-3}
10^{-2}
10^{-1}
1
10
10^{2}
10^{3}
10^{4}
P (ATM)

FIG (4)

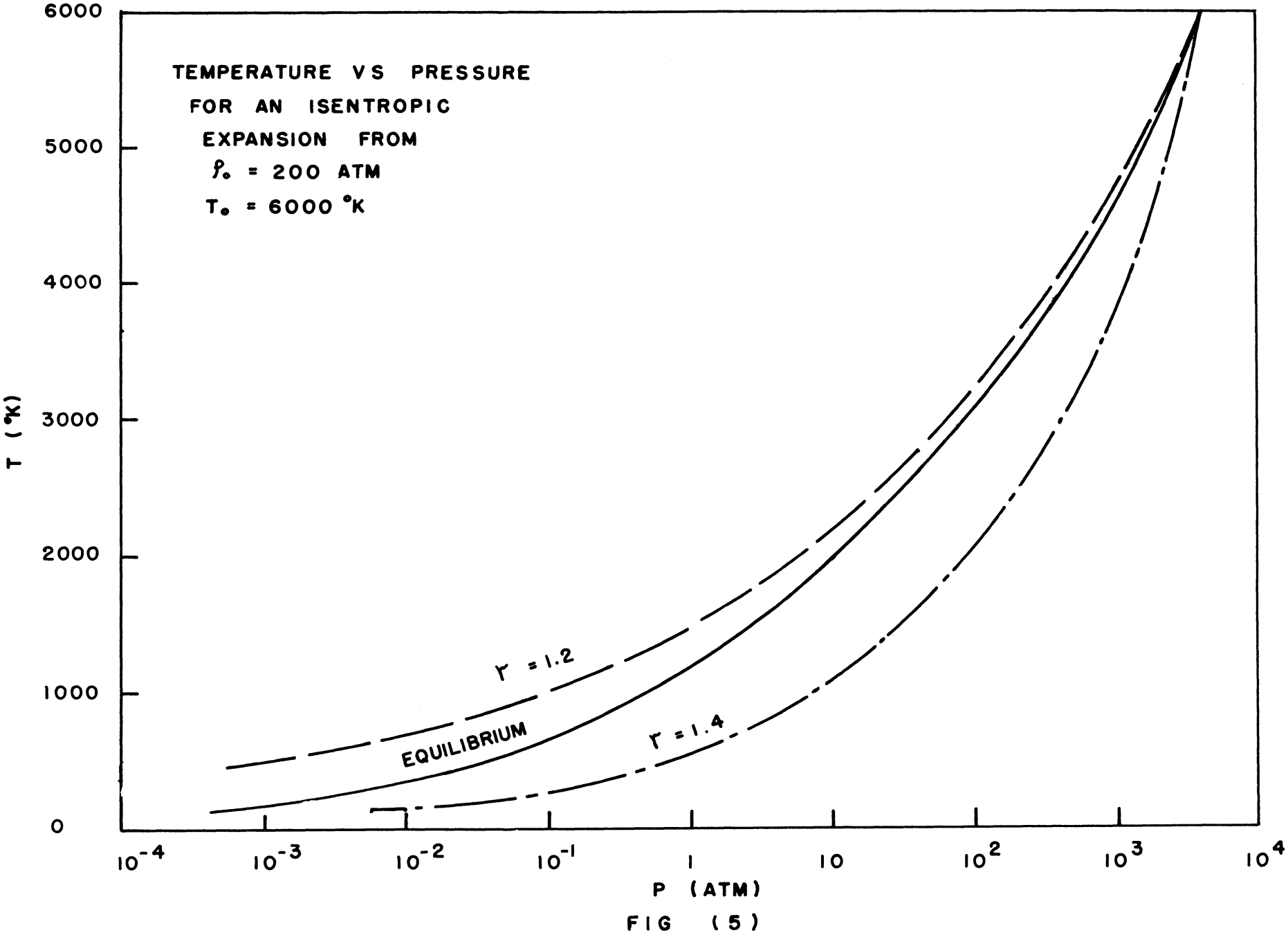
TEMPERATURE VS PRESSURE
FOR AN ISENTROPIC
EXPANSION FROM
p_o = 200 ATM
T_o = 6000 °K
6000
5000
4000
3000
2000
1000
0
T (°K)
γ = 1.2
EQUILIBRIUM
γ = 1.4
10^{-4}
10^{-3}
10^{-2}
10^{-1}
1
10
10^2
10^3
10^4
P (ATM)

FIG (5)

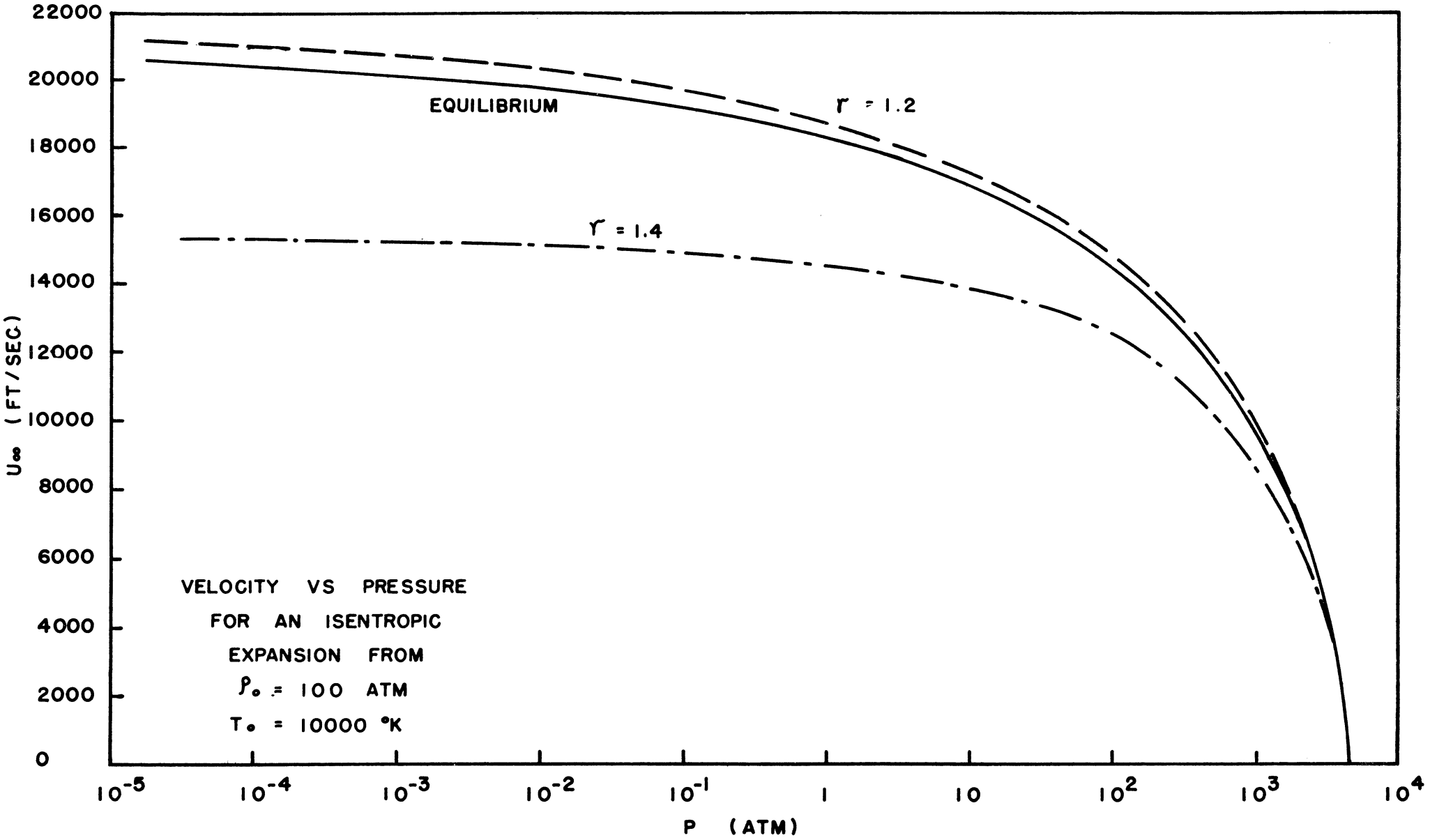
22000
20000
18000
16000
14000
12000
10000
8000
6000
4000
2000
0
U_∞ (FT/SEC)
EQUILIBRIUM
$\gamma = 1.2$
$\gamma = 1.4$
VELOCITY VS PRESSURE
FOR AN ISENTROPIC
EXPANSION FROM
$P_o = 100$ ATM
$T_o = 10000$ °K
10^{-5}
10^{-4}
10^{-3}
10^{-2}
10^{-1}
1
10
10^2
10^3
10^4
P (ATM)

FIG (6)

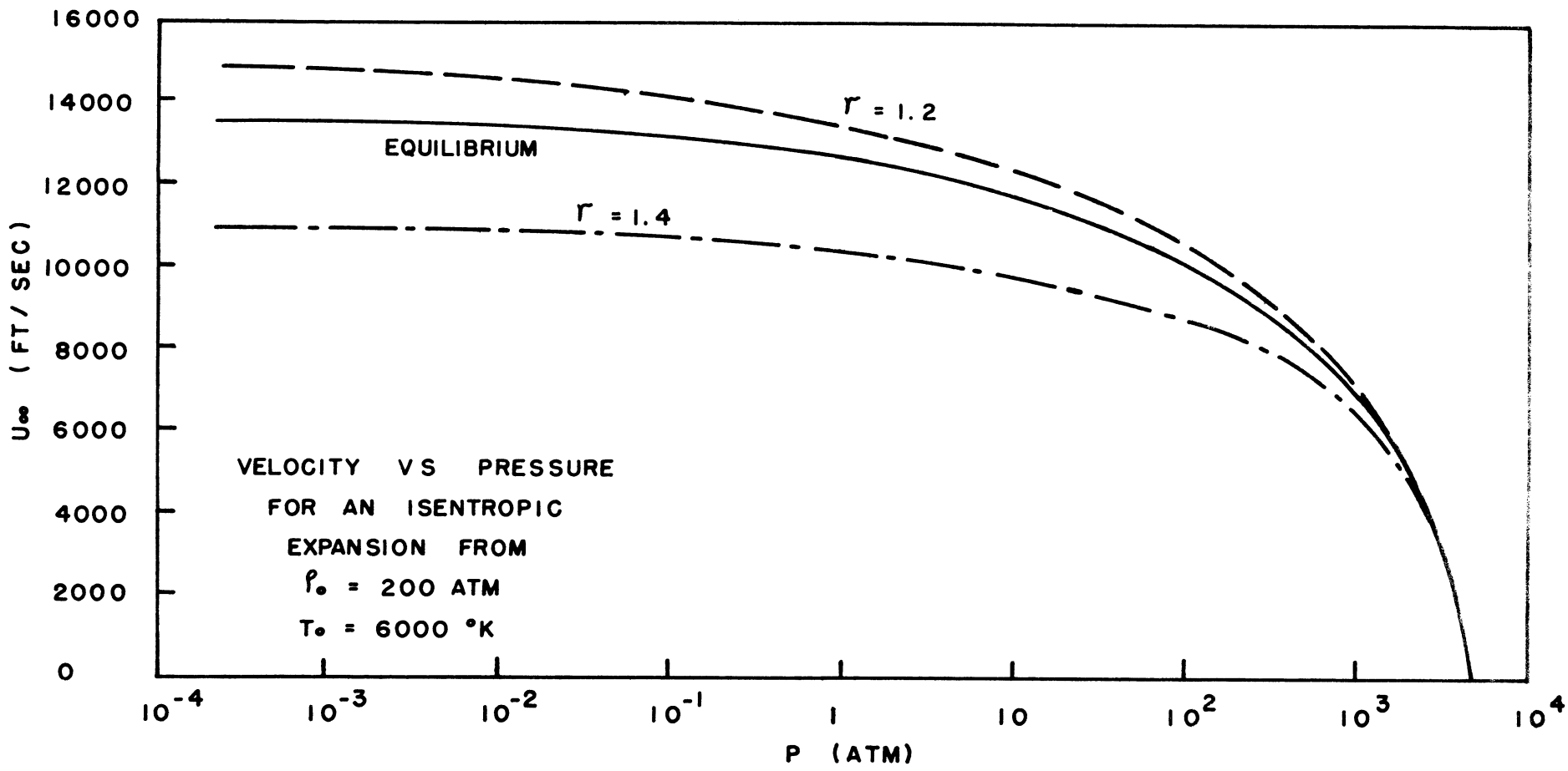
16000
14000
12000
10000
8000
6000
4000
2000
0
U_∞ (FT/SEC)
r = 1.2
EQUILIBRIUM
r = 1.4
VELOCITY VS PRESSURE
FOR AN ISENTROPIC
EXPANSION FROM
ρ_o = 200 ATM
T_o = 6000 °K
10^{-4}
10^{-3}
10^{-2}
10^{-1}
1
10
10^2
10^3
10^4
P (ATM)

FIG (7)

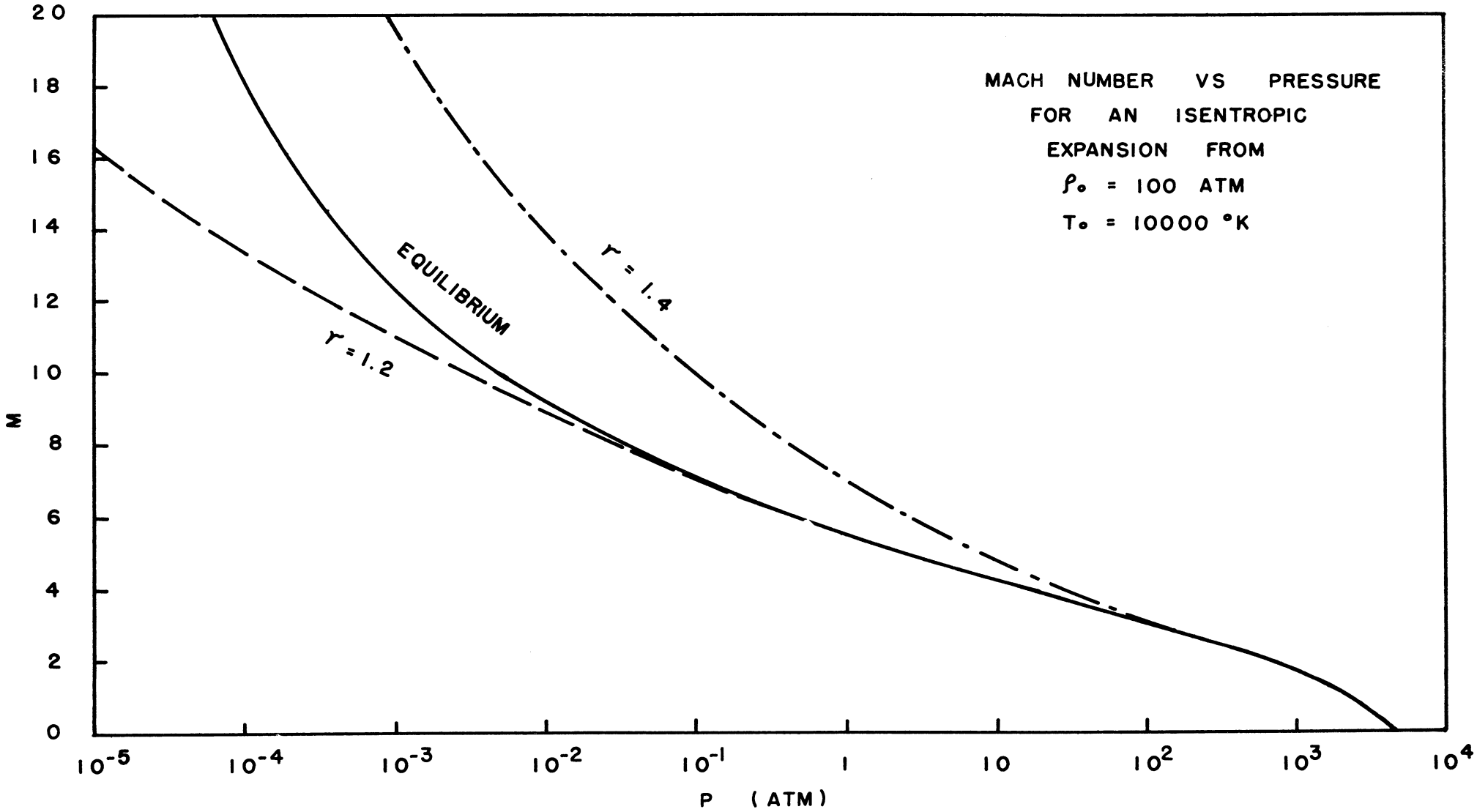
MACH NUMBER VS PRESSURE
FOR AN ISENTROPIC
EXPANSION FROM
ρ_o = 100 ATM
T_o = 10000 °K
EQUILIBRIUM
γ = 1.4
γ = 1.2
M
P (ATM)
0
2
4
6
8
10
12
14
16
18
20
10^{-5}
10^{-4}
10^{-3}
10^{-2}
10^{-1}
1
10
10^{2}
10^{3}
10^{4}

FIG (8)

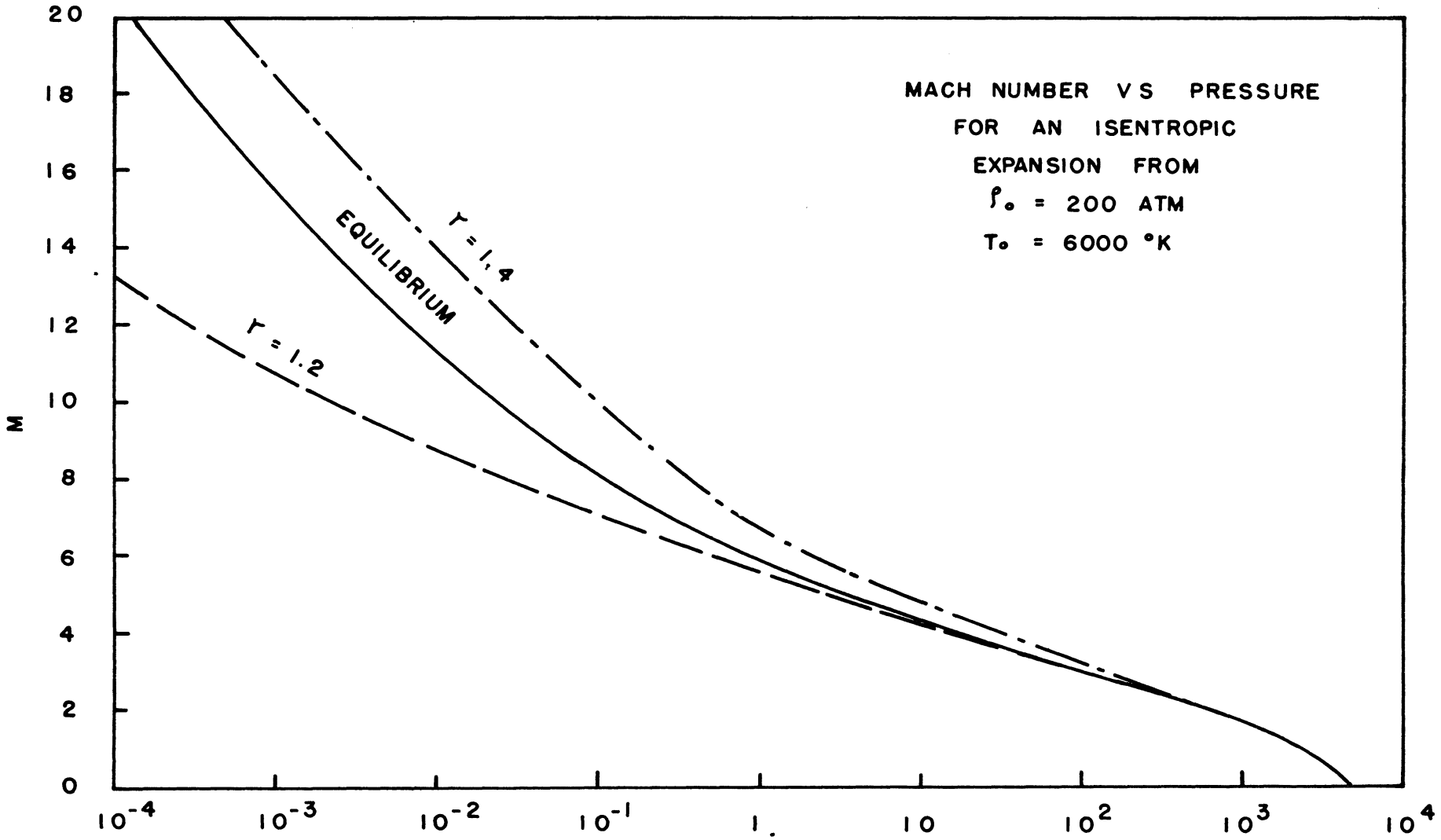
MACH NUMBER VS PRESSURE
FOR AN ISENTROPIC
EXPANSION FROM
ρ_o = 200 ATM
T_o = 6000 °K
γ = 1.4
EQUILIBRIUM
γ = 1.2
M
P (ATM)
20
18
16
14
12
10
8
6
4
2
0
10^{-4}
10^{-3}
10^{-2}
10^{-1}
1.
10
10^2
10^3
10^4

FIG (9)

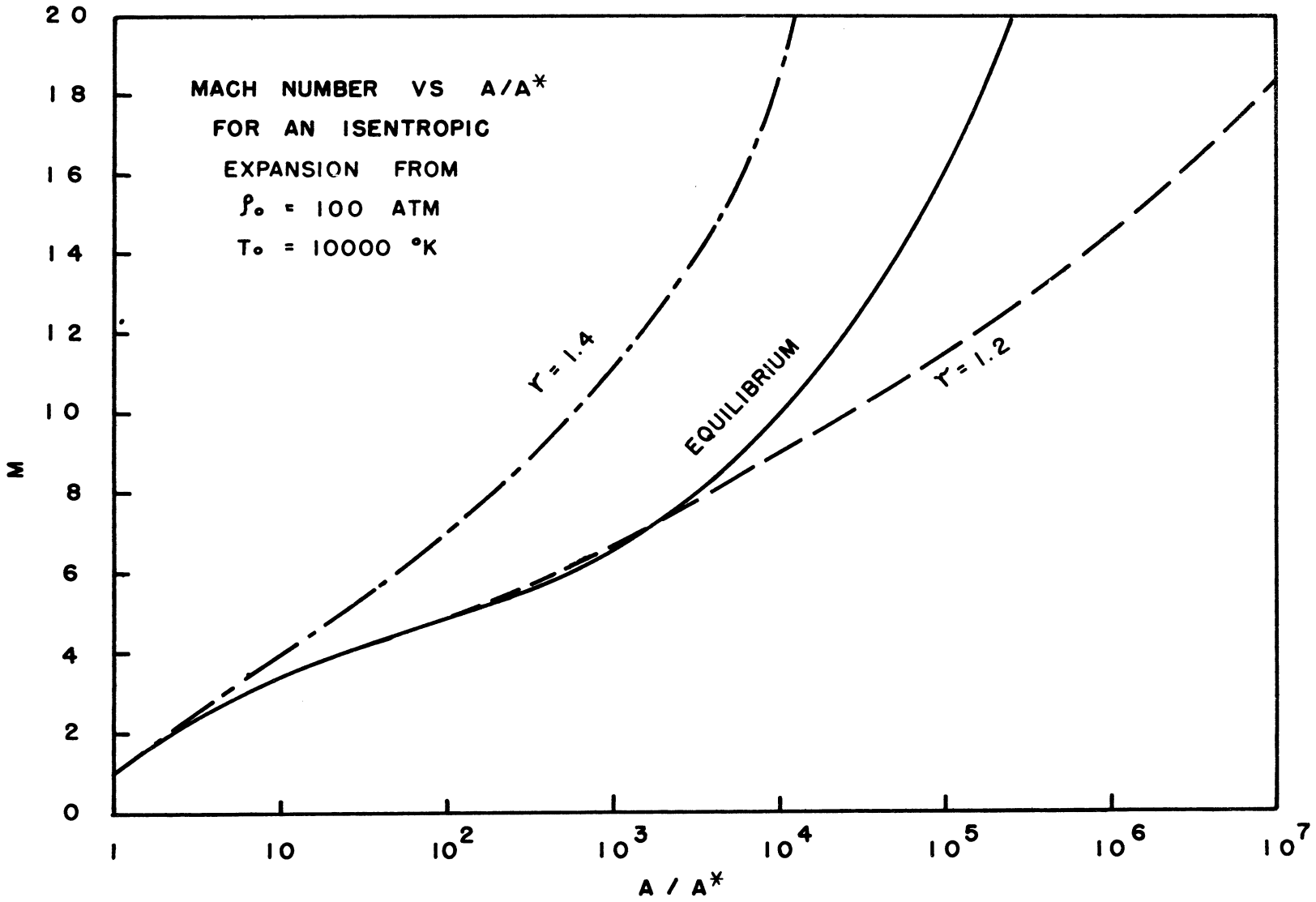
MACH NUMBER VS A/A*
FOR AN ISENTROPIC
EXPANSION FROM
ρ_o = 100 ATM
T_o = 10000 °K
γ = 1.4
EQUILIBRIUM
γ = 1.2
M
A / A*
0
2
4
6
8
10
12
14
16
18
20
1
10
10^2
10^3
10^4
10^5
10^6
10^7

FIG (10)

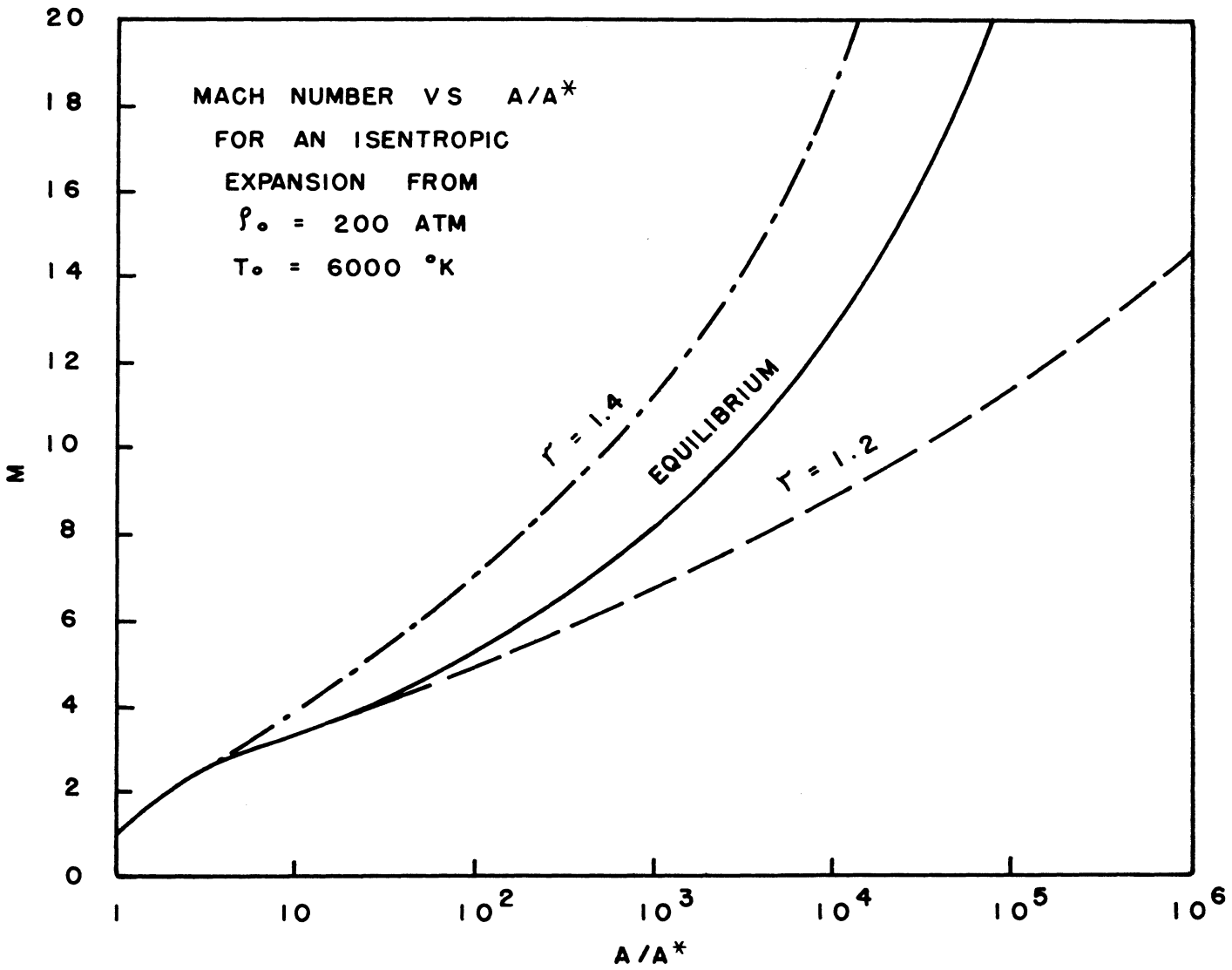
MACH NUMBER VS A/A*
FOR AN ISENTROPIC
EXPANSION FROM
ρ_o = 200 ATM
T_o = 6000 °K
γ = 1.4
EQUILIBRIUM
γ = 1.2
M
A/A*
0
2
4
6
8
10
12
14
16
18
20
1
10
10^2
10^3
10^4
10^5
10^6

FIG (11)

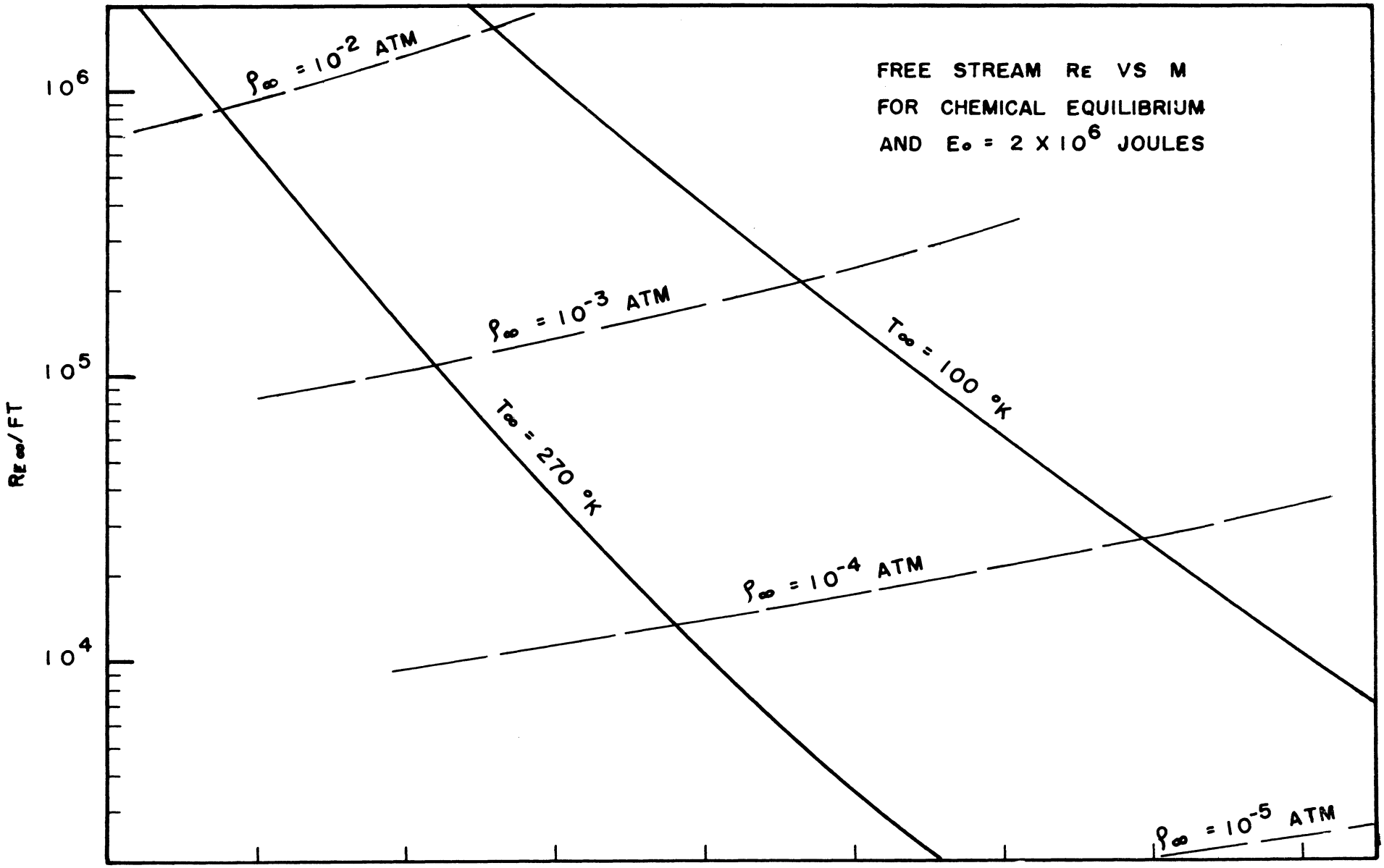
FREE STREAM RE VS M
FOR CHEMICAL EQUILIBRIUM
AND E₀ = 2 X 10⁶ JOULES
ρ∞ = 10⁻² ATM
ρ∞ = 10⁻³ ATM
ρ∞ = 10⁻⁴ ATM
ρ∞ = 10⁻⁵ ATM
T∞ = 270 °K
T∞ = 100 °K
10⁶
10⁵
10⁴
RE∞/FT
10
12
14
16
18
20
22
24
26
M∞

FIG (12)

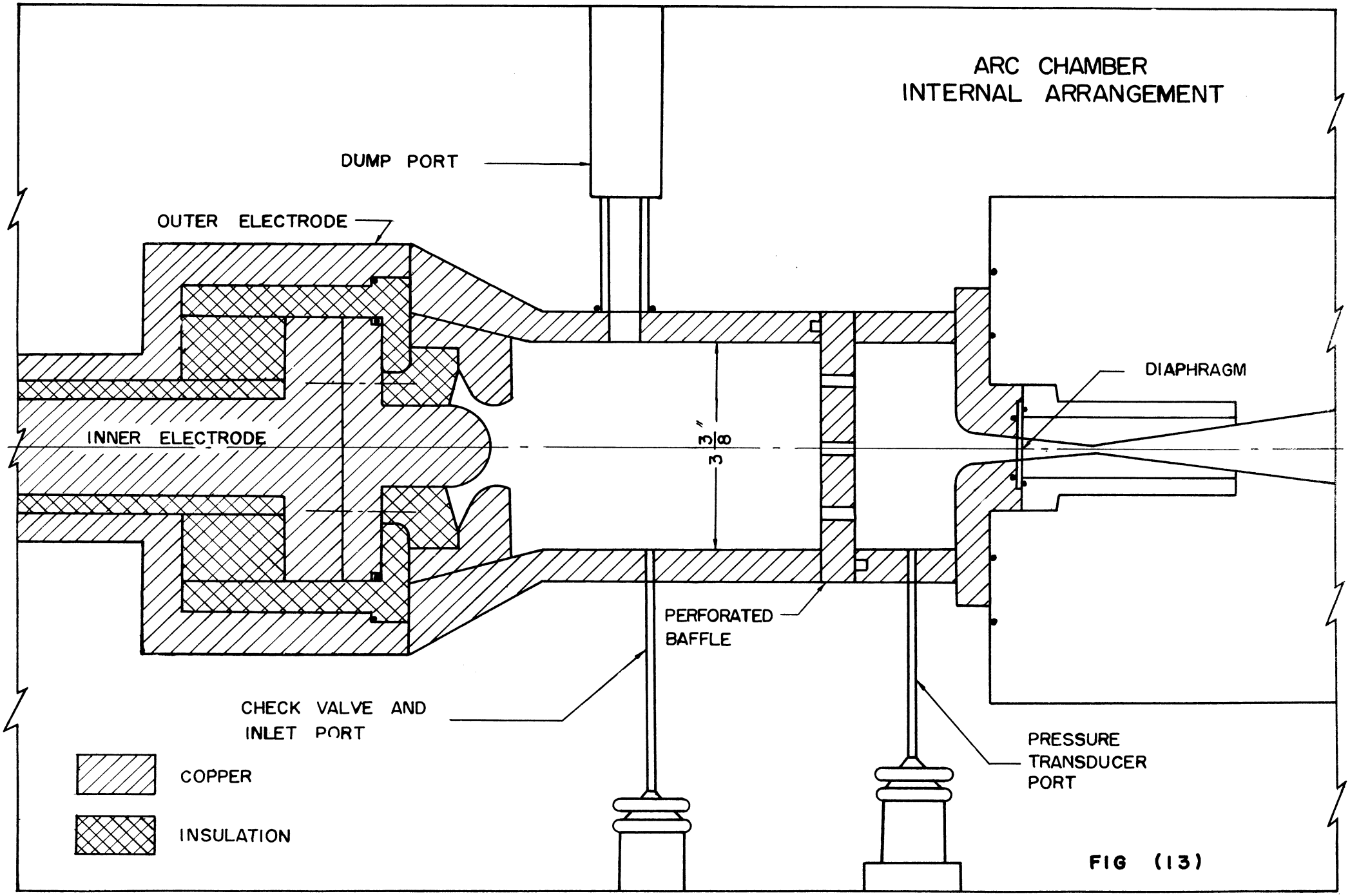
ARC CHAMBER
INTERNAL ARRANGEMENT
DUMP PORT
OUTER ELECTRODE
INNER ELECTRODE
3/8"
DIAPHRAGM
PERFORATED
BAFFLE
CHECK VALVE AND
INLET PORT
PRESSURE
TRANSDUCER
PORT
COPPER
INSULATION

FIG (13)

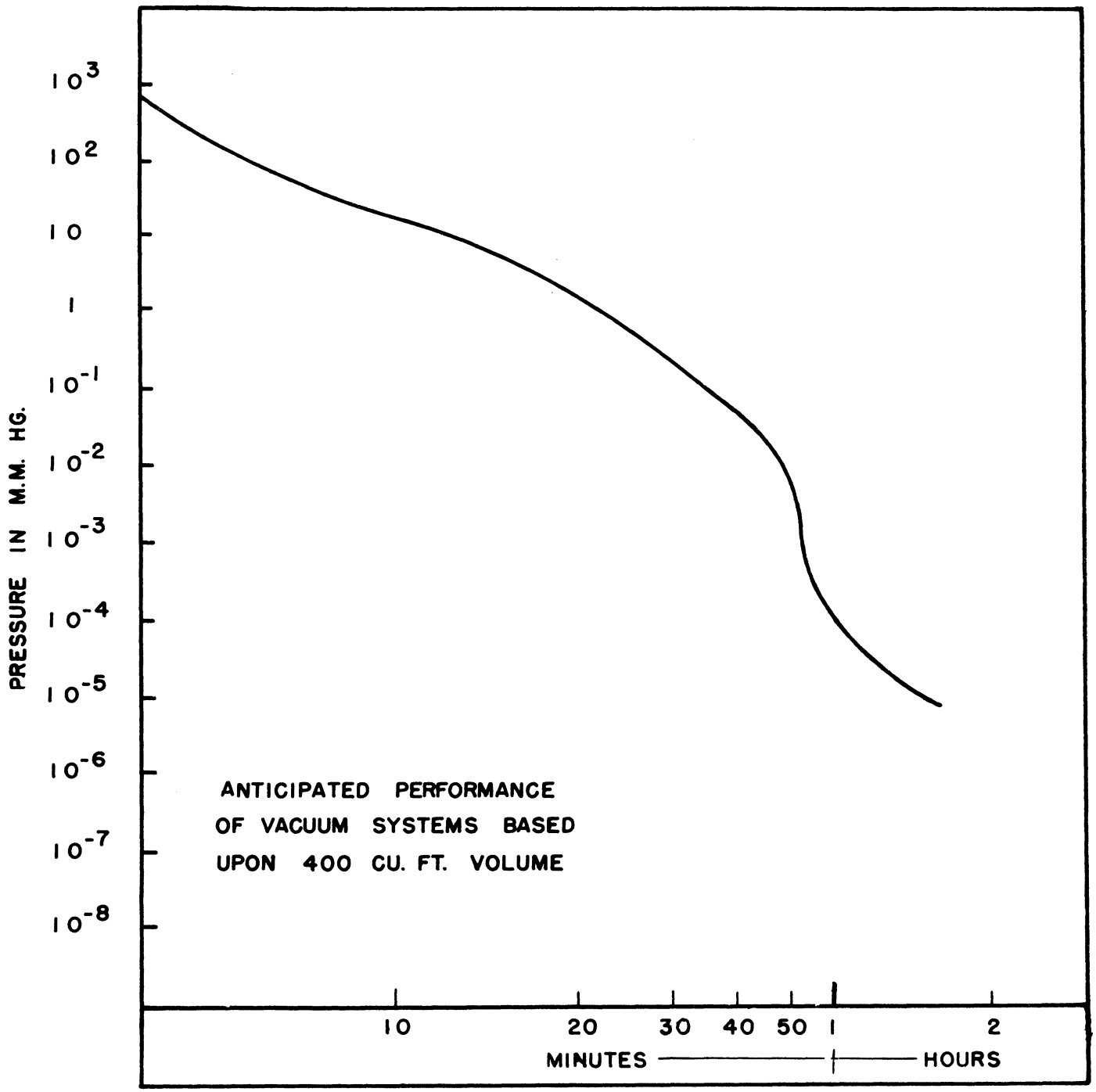
PRESSURE IN M.M. HG.
10^3
10^2
10
1
10^-1
10^-2
10^-3
10^-4
10^-5
10^-6
10^-7
10^-8
ANTICIPATED PERFORMANCE
OF VACUUM SYSTEMS BASED
UPON 400 CU. FT. VOLUME
10
20
30
40
50
1
2
MINUTES
HOURS
PUMP DOWN TIME

FIG (14)

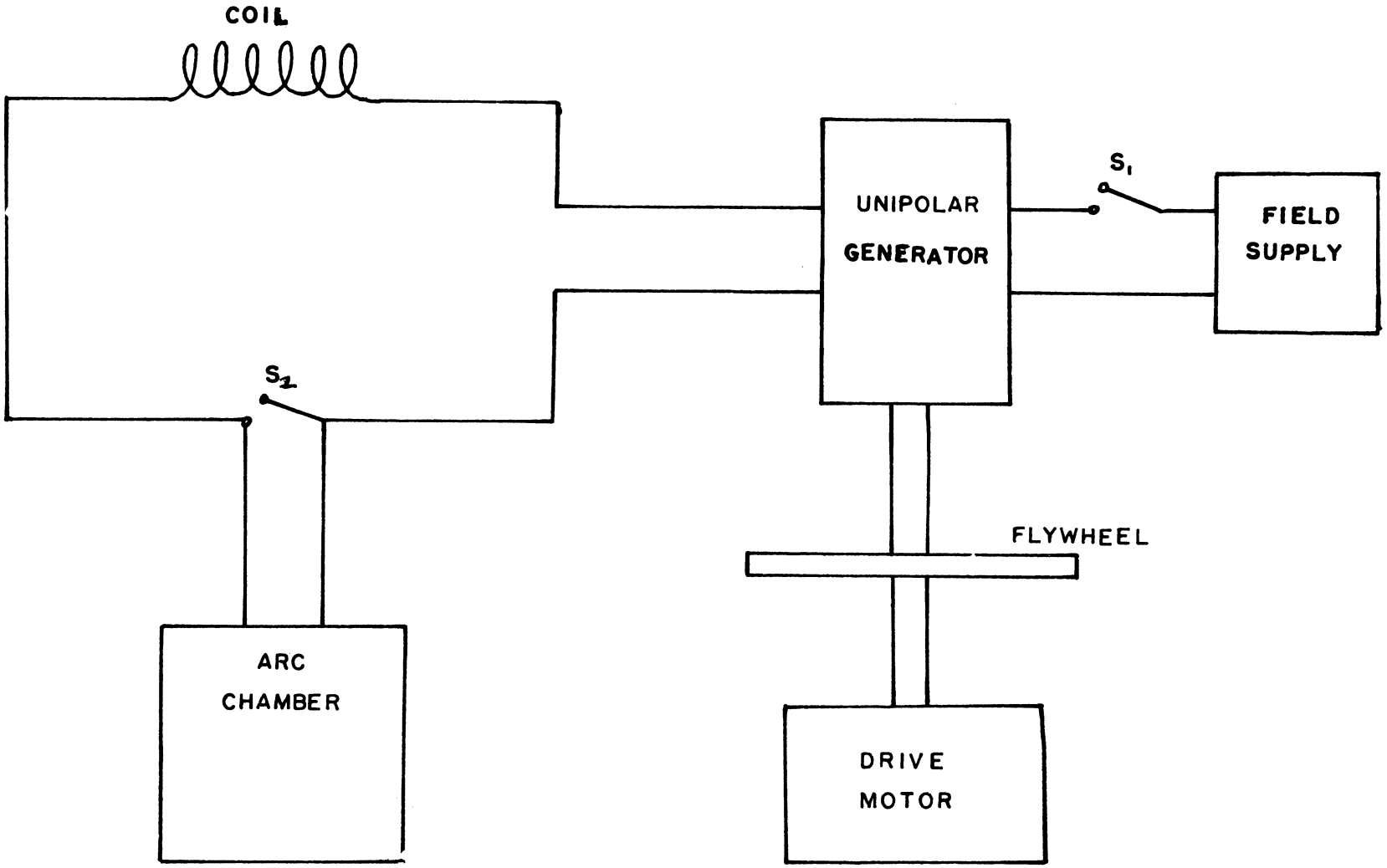

SCHEMATIC OF POWER SUPPLY

FIG (15)

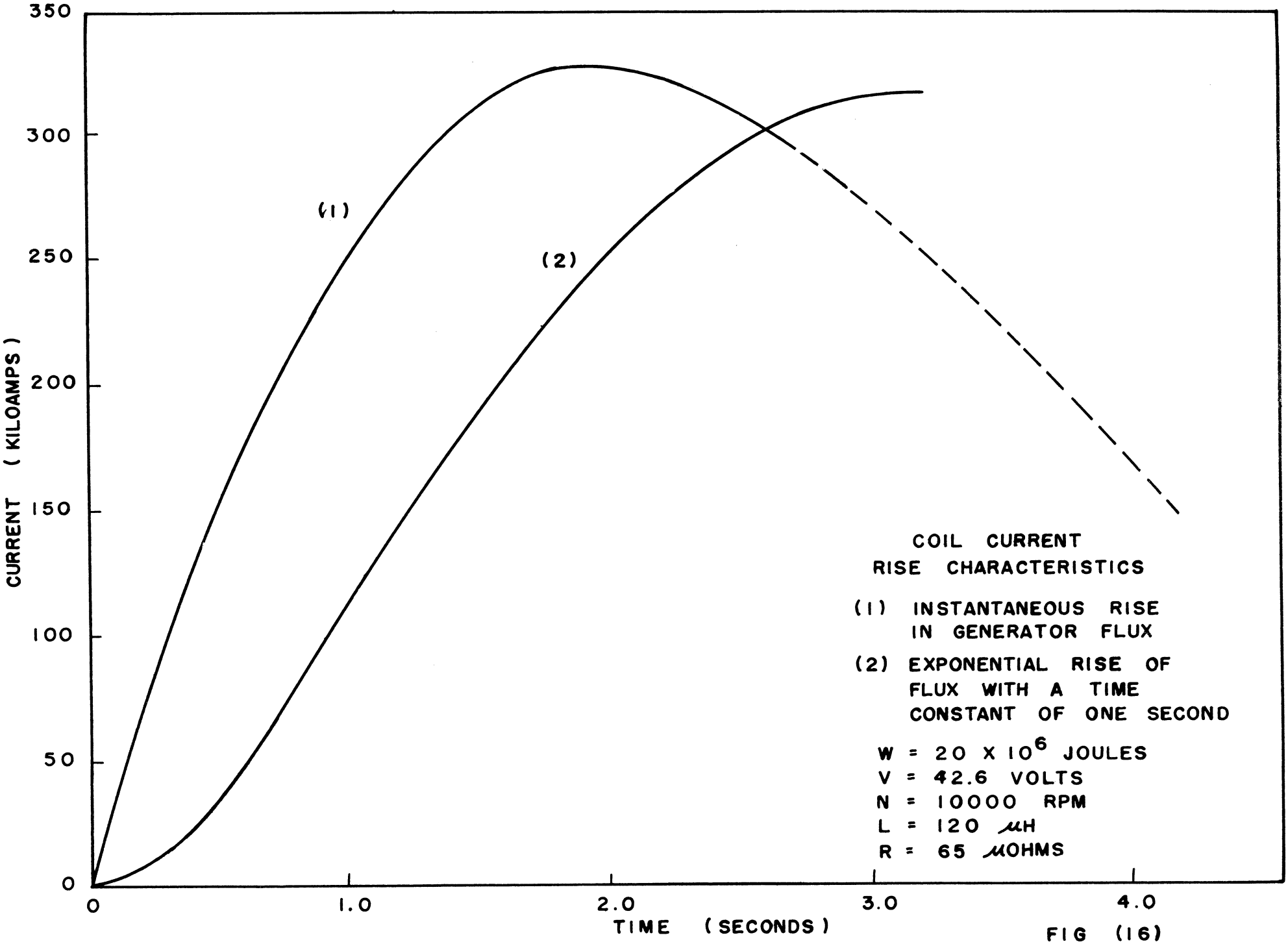
350
300
250
200
150
100
50
0
CURRENT (KILOAMPS)
(1)
(2)
0
1.0
2.0
3.0
4.0
TIME (SECONDS)
COIL CURRENT
RISE CHARACTERISTICS
(1) INSTANTANEOUS RISE
IN GENERATOR FLUX
(2) EXPONENTIAL RISE OF
FLUX WITH A TIME
CONSTANT OF ONE SECOND
W = 20 X 10^6 JOULES
V = 42.6 VOLTS
N = 10000 RPM
L = 120 μH
R = 65 μOHMS

FIG (16)

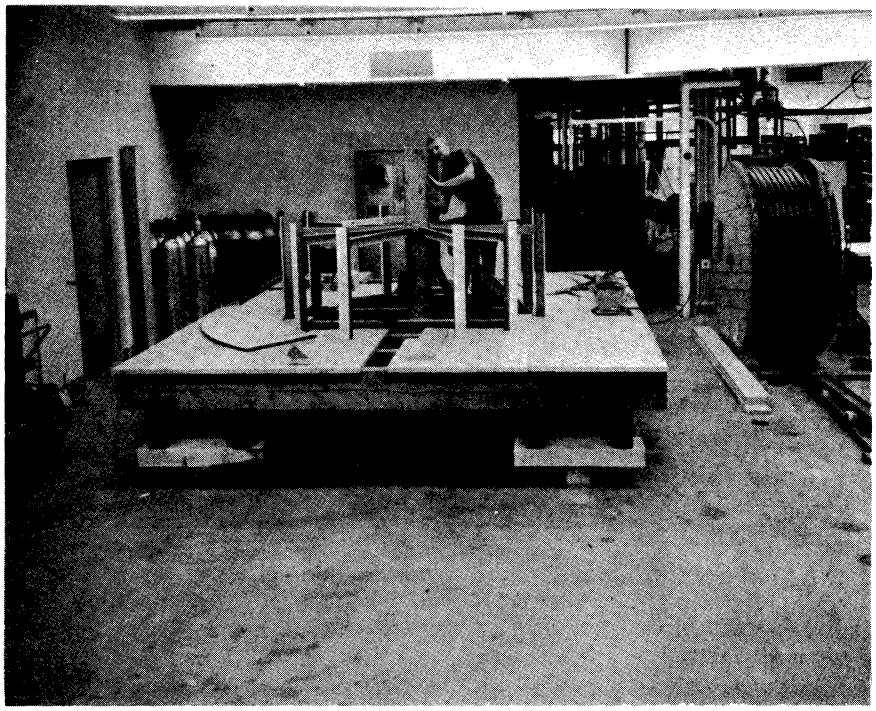

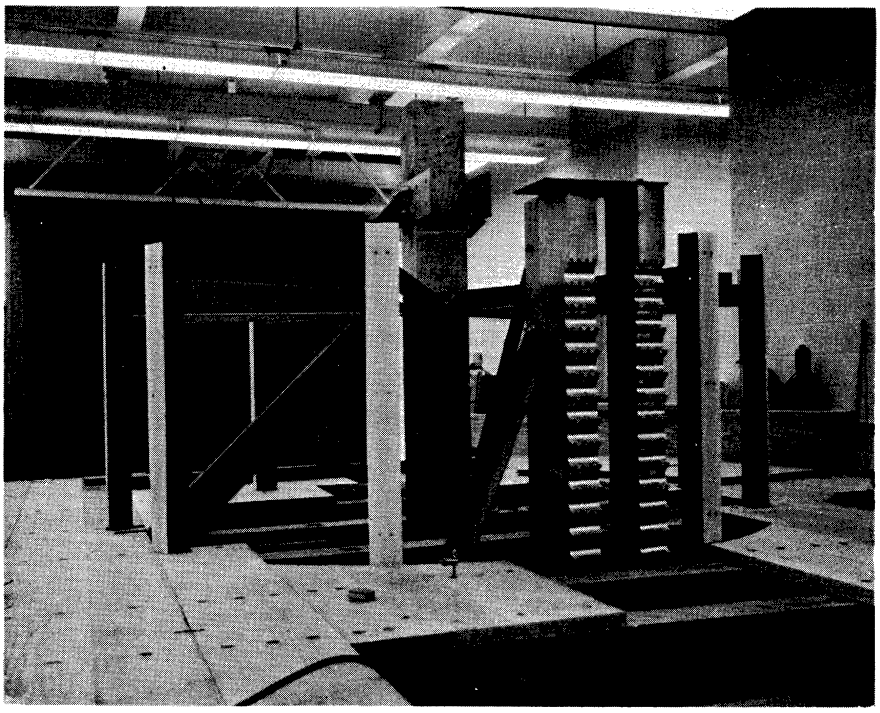

Fig. 17

DISTRIBUTION LIST

(One copy unless otherwise noted)

Chief of Naval Research
Department of the Navy
Washington 25, D.C.
Attn: Code 438 — 2
Attn: Code 419
Attn: Code 461
Attn: Code 421

Commanding Officer
Office of Naval Research
Branch Office
150 Causeway Street
Boston, Massachusetts

Commanding Officer
Office of Naval Research
Branch Office
The John Crerar Library Building
86 East Randolph Street
Chicago 1, Illinois

Commanding Officer
Office of Naval Research
Branch Office
346 Broadway
New York 13, New York

Commanding Officer
Office of Naval Research
Branch Office
1030 East Green Street
Pasadena 1, California

Commanding Officer
Office of Naval Research
Branch Office
1000 Geary Street
San Francisco 9, California

Commanding Officer
Office of Naval Research
Navy No. 100, Box 45
Fleet Post Office
New York, New York — 15

Director
Naval Research Laboratory
Washington 25, D.C.
Attn: Code 2021 — 6

Chief, Bureau of Aeronautics
Department of the Navy
Washington 25, D.C.
Attn: Research Division
Attn: Aero and Hydro Branch

Commanding Officer and Director
David Taylor Model Basin
Carderock, Maryland
Attn: Aerodynamics Laboratory

Chief, Bureau of Ordnance
Department of the Navy
Washington 25, D.C.
Attn: Code ReO
Attn: Code Re-S1-e

Commander
Dahlgren Proving Ground
Dahlgren, Virginia
Attn: Technical Library

Commander
Naval Ordnance Test Station
Inyokern, China Lake, California
Attn: Technical Library
Attn: Code 501

Commander
Naval Ordnance Laboratory
White Oak, Maryland
Attn: Hyperballistics Division
Attn: Aeroballistics Division
Attn: Aerophysics Division

Chief, Bureau of Yards and Docks
Department of the Navy
Washington 25, D.C.
Attn: Plans and Research

DISTRIBUTION LIST (Continued)

Superintendent
Naval Postgraduate School
Monterey, California

U. S. Naval Air Material
Test Center
Point Mugu, California
Attn: Chief Scientist

Commander
Air Force Office of Scientific
Research
Washington 25, D.C.
Attn: Mechanics Division

Director, Office for Advanced
Studies
Air Force Office of Scientific
Research
Box 2035
Pasadena 2, California

Commander
Western Development Division
P. O. Box 262
Inglewood, California

Commander
Air Force Cambridge Research Center
230 Albany Street
Cambridge 39, Massachusetts
Attn: Geophysical Research Library

AEDC Library
P. O. Box 162
Tullahoma, Tennessee

Commander
Wright Air Development Division
Wright-Patterson Air Force Base, Ohio
Attn: Aeronautical Research Laboratory
Attn: Aircraft Laboratory

Office of Ordnance Research
Department of the Army
Duke Station
Durham,North Carolina

Ballistic Research Laboratory
Aberdeen Proving Ground
Aberdeen, Maryland
Attn: Dr. R. H. Kent
Attn: Dr. F. D. Bennett

Internal Ballistics Laboratory
Aberdeen Proving Ground
Aberdeen, Maryland
Attn: Dr. J. H. Frazer

Commanding Officer
Redstone Arsenal
Huntsville, Alabama

Director of Research
National Aeronautics and Space
Administration
1512 H Street, N.W.
Washington 25, D.C.

Chief
Armed Forces Special Weapons Project
P. O. Box 2610
Washington 25, D.C.

Executive Secretary
Weapons System Evaluation Group
Office of the Secretary of Defense
The Pentagon
Washington 25, D.C.

Director
National Bureau of Standards
Washington 25, D.C.
Attn: Fluid Mechanics Section
Attn: Electron Physics Section

U. S. Atomic Energy Commission
Technical Information Service
Washington 25, D.C.
Attn: Technical Librarian

National Science Foundation
Division of Mathematical, Physical
and Engineering Sciences
Washington 25, D.C.

DISTRIBUTION LIST (Continued)

Documents Service Center
Armed Services Technical
Information Agency
Arlington Hall Station
Arlington 12, Virginia 5

Office of Technical Services
Department of Commerce
Washington 25, D.C.

Division of Engineering
Brown University
Providence 12, Rhode Island
Attn: Profs. Maeder, Kestin,
Probstein

Low Pressure Research Project
University of California
Engineering Field Station
1301 South 46th Street
Richmond, California

Radiation Laboratory
University of California
Livermore, California
Attn: Drs. S. A. Colgate, R. Post

Los Alamos Scientific Laboratory
University of California
Los Alamos, New Mexico
Attn: Theoretical Division (Dr. J.
L. Tuck)
Attn: Dr. R. G. Shreffler
Attn: J-1 Division (Drs. Duff, Graves)

Jet Propulsion Laboratory
California Institute of Technology
Pasadena 4, California
Attn: Dr. P. Wegener

Guggenheim Aeronautical Laboratory
California Institute of Technology
Pasadena 4, California
Attn: Prof. C. B.Millikan, Director
Attn: Prof. L. Lees
Attn: Prof. H. W. Liepmann

Department of Physics
California Institute of Technology
Pasadena 4, California
Attn: Prof. F. Zwicky

Department of Aerodynamics
Case Institute of Technology
Cleveland 6, Ohio
Attn: Prof. G. Kuerti

Yerkes Observatory
University of Chicago
Williams Bay, Wisconsin
Attn: Prof. S. Chandrasekhar

Graduate School of Aeronautical
Engineering
Cornell University
Ithaca, New York
Attn: Prof. W. Sears
Attn: Prof. E. L. Resler, Jr.

Cornell Aeronautical Laboratory
4455 Genesse Street
Buffalo, New York
Attn: Dr. A. Bertzberg

Department of Engineering Sciences
Harvard University
Cambridge 38, Massachusetts
Attn: Prof. G. Carrier
Attn: Prof. H. Emmons

Harvard Observatory
Harvard University
Cambridge, Massachusetts
Attn: Prof. F. Whipple

Department of Aeronautical
Engineering
University of Illinois
Urbana, Illinois
Attn: Prof. H. S. Stillwell, Chairman

Chance-Vought Aircraft Corporation
Dallas, Texas

DISTRIBUTION LIST (Continued)

Department of Aeronautics
Johns Hopkins University
Balitmore 18, Maryland
Attn: Prof. F. H. Clauser

Applied Physics Laboratory
Johns Hopkins University
P. O. Box 244, Route 1
Laurel, Maryland
Attn: Technical Reports Office

Department of Physics
Lehigh University
Bethlehem, Pennsylvania
Attn: Prof. R. J. Emrich

Institute of Fluid Mechanics and
Applied Mathematics
University of Maryland
College Park, Maryland
Attn: Profs. Burgers, Pai

Department of Mathematics
Massachusetts Institute of Technology
Cambridge 39, Massachusetts
Attn: Prof. C. C. Lin

Department of Mechanical Engineering
Massachusetts Institute of Technology
Cambridge 39, Massachusetts
Attn: Prof. J. Kaye

Department of Aeronautical Engineering
The University of Michigan
Ann Arbor, Michigan
Attn: Prof. W. C. Nelson

The University of Michigan Research
Institute
The University of Michigan
Ann Arbor, Michigan
Attn: Prof. O. Laporte
Attn: Prof. G. Uhlenbeck

The Department of Astronomy
The University of Michigan
Ann Arbor, Michigan
Attn: Prof. L. Goldberg

Department of Aeronautical Engineering
University of Minnesota
Minneapolis, Minnesota
Attn: Prof. J. D. Akerman, Chairman

Institute of Meteororitics
University of New Mexico
Albuquerque, New Mexico
Attn: Prof. L. LaPaz

Institute for Mathematics and
Mechanics
New York University
25 Waverly Place
New York 3, New York
Attn: Prof. R. Courant, Director

Guggenheim School of Aeronautics
New York University
New York 53, New York
Attn: Prof. J. F. Ludloff

Department of Mechanical Engineering
Northwestern University
Evanston, Illinois
Attn: Prof. A. B. Cambel

Department of Physics
University of Oklahoma
Norman, Oklahoma
Attn: Prof. R. G. Fowler

Aerodynamics Laboratory
Polytechnic Institute of Brooklyn
Freeport, Long Island, New York
Attn: Prof. A. Ferri

Palmer Physics Laboratory
Princeton University
Princeton, New Jersey
Attn: Prof. W. Bleakney

Engineering Center
University of Southern California
University Park
Los Angeles 7, California
Attn: Dr. R. Chuan

DISTRIBUTION LIST (Continued)

Department of Aeronautical Engineering
Princeton University
Princeton, New Jersey
Attn: Profs. S. Bogdonoff, W. Hayes

Princeton University Observatory
Princeton, New Jersey
Attn: Prof. L. Spitzer, Jr.

Department of Aeronautical Engineering
Rensselaer Polytechnic Institute
Troy, New York
Attn: Prof. R. P. Harrington

Guggenheim Aeronautical Laboratory
Stanford University
Stanford, California

Defense Research Laboratory
University of Texas
P. O. Box 8029
Austin, Texas
Attn: M. J. Thompson

College of Engineering
University of California at
Los Angeles
Los Angeles 24, California
Attn: Prof.J. Kaplan

Department of Physics
University of California at
Los Angeles
Los Angeles 24, California
Attn: Prof. J. Kaplan

Experimental Research Group
University of Utah
Salt Lake City, Utah
Attn: Prof. M. A. Cook, Director

Department of Aeronautical Engineering
University of Washington
Seattle 5, Washgington
Attn: Department Librarian

Sandia Corporation, Sandia Base
Albuquerque, New Mexico

Department of Chemistry
University of Wisconsin
Madison, Wisconsin
Attn: Prof. J. O. Hirschfelder

Aerojet Engineering Corporation
6352 N. Irwindale Avenue, Box 296
Azusa, California

ARO, Inc.
Tullahoma, Tennessee
Attn: Dr. R. W. Perry, Mr. R. Smelt

AVCO Manufacturing Company
Research Laboratories
2385 Revere Beach Parkway
Everett 49, Massachusetts
Attn: Drs. Kantrowitz, Lin;
Miss Spence, Librarian

Flight Sciences Laboratory, Inc.
1965 Sheridan Drive
Buffalo 23, New York
Attn: Dr. J. S. Isenberg, Technical
Director

Boeing Airplane Company
Box 3107
Seattle 14, Washington

Convair
San Diego Division
San Diego, California
Attn: Dr. W. H. Dorrance

Douglas Aircraft Company, Inc.
3000 Ocean Park Boulevard
Santa Monica, California

Sterlin Chemical Laboratory
Yale University
New Haven, Connecticut
Attn: Prof. J. G. Kirkwood

Fairchild Engine Division
Fairchild Engine and Aircraft Company
Farmingdale, Long Island, New York
Attn: Mrs. C. Minck, Librarian

DISTRIBUTION LIST (Continued)

Fairchild Engine and Aircraft Company
Guided Missiles Division
Wyabdanch, Long Island, New York

General Electric Company
Research Laboratory
P. O. Box 1088
Schenectady, New York
Attn: Drs. Nagamatsu, White, Alpher

The Glenn L. Martin Company
Department 520, Mail No. 3072
Baltimore 3, Maryland
Attn: Mr. L. Cooper

Grumman Aircraft
Engineering Corporation
Bethpage, Long Island, New York

Hughes Aircraft Corporation
Research and Development Laboratory
Culver City, California
Attn: Dr. A. E. Puckett

Lockheed Aircraft Missile Systems
Division
Van Nuys, California
Attn: Dr. L. Ridenour

Marquardt Aircraft Corporation
7801 Havenhurst
Van Nuys, California

Midwest Research Institute
Department of Physics
4049 Pennsylvania Avenue
Kansas City, Missouri
Attn: Mr. K. L. Sandefur

General Electric Company
Special Defense Projects Department
3198 Chestnut Street
Philadelphia 4, Pennsylvania
Attn: Drs. R. J. Kirby, J. W. Bond, Jr.,
Y.A. Yoles (Thermodynamics Section)
Attn: Aerophysics Laboratory Operation

Northrop Aircraft, Inc.
Northrop Field
Hawthorne, California

Ramo-Woolridge Corporation
8820 Bellance Avenue
Los Angeles 45, California
Attn: Dr. M. U. Clauser

RAND Corporation
1700 Main Street
Santa Monica, California
Attn: E. P. Williams, C. Gazley, Jr.

Republic Aviation Corporation
Farmingdale, Long Island, New York

Stanford Research Institute
Poulter Laboratories
Stanford, California
Attn: Drs. Poulter,Duvall, Doll

United Aircraft Corporation
Research Department
362 Main Street
East Hartford 8, Connecticut

Borg-Warner Corporation
Research Center
Applied Physics Group
Des Plaines, Illinois
Attn: Mr. Roy J. Heyman

North American Aviation, Inc.
Aerophysics Department
12214 Lakewood Boulevard
Downey, California
Attn: Dr. van Driest

Dr. R. H. Thomas
Harvard University
Cambridge 38, Massachusetts

Professor A. H. Taub
University of Illinois
Urbana, Illinois

DISTRIBUTION LIST (Continued)

Dr. C. W. Lampson
Terminal Ballistics Laboratory
Aberdeen Proving Ground
Aberdeen, Maryland

Director
National Bureau of Standards
Washington, D.C.
Attn: Pneumatic Laboratory,
Thermodynamics Section

Dr. E. C. Noonan
Fuels and Propellants Division
Naval Ordnance Laboratory
White Oak, Maryland

Dr. S. J. Jacobs
Detonation Division
Naval Ordnance Laboratory
White Oak, Maryland

Professor A. B. Arons
Department of Physics
Amherst University
Amherst, Massachusetts

Professor N. R. Davidson
Department of Chemistry
California Institute of Technology
Pasadena 4, California

Professor S. S. Penner
Department of Jet Propulsion
California Institute of Technology
Pasadena 4, California

Dr. R. N. Hollyer
Research Staff
The General Motors Corporation
P. O. Box 188, North End Station
Detroit 2, Michigan

Professor H. C. Hottell
Department of Fuel Engineering
Massachusetts Institute of Technology
Cambridge 39, Massachusetts

Professor R. G. Stoner
Department of Physics
Pennsylvania State University
University Park, Pennsylvania

Professor H. G. Lew
Department of Aeronautical Engineering
Pennsylvania State University
University Park, Pennsylvania

American Machine and Foundry Company
1104 S. Wabash Avenue
Chicago 5, Illinois
Attn: Mechanics Research Department

Therm Advanced Research
Therm, Inc.
Ithaca, New York
Attn: Dr. A. Ritter

Director
National Bureau of Standards
Washington 25, D.C.
Attn: Electron Physics Branch,
Dr. L. L. Marton

Mr. K. M. Siegel
Upper Atmosphere Section
Willow Run Research Center
The University of Michigan
Ypsilanti, Michigan

Professor A. H. Kuthlthau
Department of Physics
University of Virginia
Charlottesville, Virginia

Commanding Officer and Director
U. S. Naval Civil Engineering Laboratory
Port Hueneme, California
Attn: Code L54

Professor H. Cohen
IBM Research Center
P. O. Box 218
Yorktown Heights, New York

DISTRIBUTION LIST (Concluded)

Australian Weapons Research
Establishment
c/o Defense Research and Development
Representative
Australian Joint Service Staff
P. O. Box 4837
Washington 8, D.C.

Hydronautics, Inc.
200 Monroe Street
Rockville, Maryland
Attn: Messrs. P. Eisenberg,
M. P. Tulin

Institute of Aerophysics
University of Toronto
Toronto, Canada
Attn: Dr. G. N. Patterson, Director

Division of Mechanical Engineering
National Research Foundation
Ottawa, Canada
Attn: Dr. J. Lukasiewicz

Dr. Y. V. G. Acharya, Assistant
Director
National Aeronautical Laboratory
Palace Grounds, Jayamahal Road
Bangalore-1, India